

Universidad de Málaga

Málaga, 15 Diciembre 2014

Métodos ADER-WENO en volúmenes finitos
aplicados a la resolución de problemas hiperbólicos
en mallados con refinamiento adaptativo.

Arturo Hidalgo

Universidad Politécnica de Madrid.

*Joint work with Michael Dumbser y Olindo Zanotti
(Università degli Studi di Trento, Italy).*



CONTENTS

- 1. Motivation.**
- 2. Mathematical formulation.**
- 3. WENO reconstruction.**
- 4. Local-Space time DG.**
- 5. Adaptive Mesh Refinement.**
- 6. Numerical examples.**

MOTIVATION

Many problems related to fluid dynamics can be represented by systems of conservation laws.

Very often, different temporal and spatial scales are involved (e.g. astrophysics).

In these situations Adaptive Mesh Refinement (AMR), dynamic change of the computational grid, becomes necessary.

One of the first references in AMR:

Berger & Colella (1989), “Local adaptive mesh refinement for shock hydrodynamics”, JCP , 82, 64-84.

References in AMR+High Order:

Colella et al (2009), “High order adaptive methods on locally rectangular grids”, JPCS , 180, 012010.

Burger et al. (2012) “Spectral WENO schemes with Adaptive Mesh refinement for models of polydisperse sedimentation”, ZAMM, 93, (6-7)

Mignone et al. (2012) “The Pluto code for Adaptive Mesh Computations in astrophysical uid dynamics”, ApJ Suppl., 198, 7.

ADER schemes, very useful technique to achieve high order:
in time in a single time step.

Original version: use the Lax-Wendroff procedure [Toro et al. (2001); Titarev and Toro (2002) ...]

- Modern version: use a weak integral formulation of the governing PDE
[Dumbser et al. (2008) JCP, 227, 3971]

AMR+ADER+WENO schemes.

Dumbser, Zanotti, Hidalgo, Balsara (2013) 'ADER-WENO Finite Volume schemes with space-time adaptive mesh refinement' JCP, 248, 257-286

MATHEMATICAL FORMULATION

We consider the 3D-hyperbolic system of balance laws in Cartesian coordinates

$$\frac{\partial \mathbf{u}}{\partial t} + \frac{\partial \mathbf{f}}{\partial x} + \frac{\partial \mathbf{g}}{\partial y} + \frac{\partial \mathbf{h}}{\partial z} = \mathbf{S}(\mathbf{u}, \mathbf{x}, t)$$

MATHEMATICAL FORMULATION

We consider the 3D-hyperbolic system of balance laws in Cartesian coordinates

$$\frac{\partial \mathbf{u}}{\partial t} + \frac{\partial \mathbf{f}}{\partial x} + \frac{\partial \mathbf{g}}{\partial y} + \frac{\partial \mathbf{h}}{\partial z} = \mathbf{S}(\mathbf{u}, \mathbf{x}, t)$$

and carry out a finite volume discretization

$$\begin{aligned} \mathbf{u}_{ijk}^{n+1} = & \mathbf{u}_{ijk}^n + \frac{\Delta t}{\Delta x_i} (\mathbf{f}_{i+1/2,j,k} - \mathbf{f}_{i-1/2,j,k}) + \frac{\Delta t}{\Delta y_j} (\mathbf{g}_{i,j+1/2,k} - \mathbf{g}_{i,j-1/2,k}) + \\ & + \frac{\Delta t}{\Delta z_k} (\mathbf{h}_{i,j,k+1/2} - \mathbf{h}_{i,j,k-1/2}) = \Delta t \mathbf{S}_{ijk} \end{aligned}$$

Where we have integrated over the control volumes

$$I_{ijk} = [x_{i-1/2}, x_{i+1/2}] \times [y_{j-1/2}, y_{j+1/2}] \times [z_{k-1/2}, z_{k+1/2}]$$

where

$$u_{ijk}^n = \frac{1}{\Delta x_i} \frac{1}{\Delta y_j} \frac{1}{\Delta z_k} \int_{x_{i-1/2}}^{x_{i+1/2}} \int_{y_{j-1/2}}^{y_{j+1/2}} \int_{z_{k-1/2}}^{z_{k+1/2}} u(x, y, z, t^n) dz dy dx$$

$$\mathbf{f}_{i+1/2,j,k} = \frac{1}{\Delta t} \frac{1}{\Delta y_j} \frac{1}{\Delta z_k} \int_{t^n}^{t^{n+1}} \int_{y_{j-1/2}}^{y_{j+1/2}} \int_{z_{k-1/2}}^{z_{k+1/2}} \tilde{\mathbf{f}}(\mathbf{q}_h^-(x_{i+1/2}, y, z, t), \mathbf{q}_h^+(x_{i+1/2}, y, z, t^n)) dz dy dt$$

$$\mathbf{g}_{i,j+1/2,k} = \frac{1}{\Delta t} \frac{1}{\Delta x_i} \frac{1}{\Delta z_k} \int_{t^n}^{t^{n+1}} \int_{x_{i-1/2}}^{x_{i+1/2}} \int_{z_{k-1/2}}^{z_{k+1/2}} \tilde{\mathbf{g}}(\mathbf{q}_h^-(x, y_{j+1/2}, z, t), \mathbf{q}_h^+(x, y_{j+1/2}, z, t)) dz dx dt$$

$$\mathbf{h}_{i,j,k+1/2} = \frac{1}{\Delta t} \frac{1}{\Delta x_i} \frac{1}{\Delta y_j} \int_{t^n}^{t^{n+1}} \int_{x_{i-1/2}}^{x_{i+1/2}} \int_{y_{j-1/2}}^{y_{j+1/2}} \tilde{\mathbf{h}}(\mathbf{q}_h^-(x, y, z_{k+1/2}, t), \mathbf{q}_h^+(x, y, z_{k+1/2}, t)) dy dx dt$$

$$\mathbf{S}_{ijk} = \frac{1}{\Delta t} \frac{1}{\Delta x_i} \frac{1}{\Delta y_j} \frac{1}{\Delta z_k} \int_{t^n}^{t^{n+1}} \int_{x_{i-1/2}}^{x_{i+1/2}} \int_{y_{j-1/2}}^{y_{j+1/2}} \int_{z_{k-1/2}}^{z_{k+1/2}} \mathbf{S}(x, y, z, t) dz dy dx dt$$

where \mathbf{q}_h is a space-time predictor.

Numerical flux

1) Local Lax-Friedrichs numerical flux:

$$\tilde{f}(\mathbf{q}_h^-, \mathbf{q}_h^+) = \frac{1}{2}(\mathbf{f}(\mathbf{q}_h^+) + \mathbf{f}(\mathbf{q}_h^-)) + \frac{1}{2} |s_{\max}| (\mathbf{q}_h^+ - \mathbf{q}_h^-)$$

where $|s_{\max}|$ denotes the maximum eigenvalue of the Jacobian Matrix $\mathbf{A} = \partial \mathbf{f} / \partial \mathbf{u}$

2) Osher-type numerical flux (*):

$$\tilde{f}(\mathbf{q}_h^-, \mathbf{q}_h^+) = \frac{1}{2}(\mathbf{f}(\mathbf{q}_h^+) + \mathbf{f}(\mathbf{q}_h^-)) + \frac{1}{2} \left(\int_0^1 |\mathbf{A}(\psi(s))| ds \right) (\mathbf{q}_h^+ - \mathbf{q}_h^-)$$

$$\psi(s) = \psi(\mathbf{q}_h^-, \mathbf{q}_h^+, s) = \mathbf{q}_h^- + s(\mathbf{q}_h^- + \mathbf{q}_h^+)$$

(*) Variant of the Osher-Solomon flux proposed in:

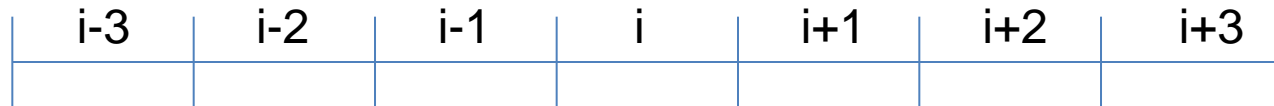
M. Dumbser, E.F. Toro, On universal Osher-type schemes for general nonlinear hyperbolic conservation laws, Communications in Computational Physics 10 (2011) 635-671.

MAIN INGREDIENTS:

- High-order reconstruction of fluxes at cell interfaces, achieved using Weighted Essentially Non Oscillatory (WENO) reconstruction.
- High-order evolution in time, using ADER-LSTDG approach.

WENO RECONSTRUCTION

$$\mathcal{S}_{ijk}^{s,x} = \bigcup_{e=i-L}^{i+R} I_{ejk}, \mathcal{S}_{ijk}^{s,y} = \bigcup_{e=j-L}^{j+R} I_{iek}, \mathcal{S}_{ijk}^{s,z} = \bigcup_{e=k-L}^{k+R} I_{ije}$$



M=even
(M=2)



Three stencils



M=odd
(M=3)



Four stencils



M+1 cells in each stencil

1) We perform WENO reconstruction in **x direction**

$$\mathbf{w}_h^{s,x}(\mathbf{x}, t^n) = \sum_{p=0}^M \psi_p(\xi) \hat{\mathbf{w}}_{ijk,p}^{n,s} := \psi_p(\xi) \hat{\mathbf{w}}_{ijk,p}^{n,s}, \quad \forall \mathcal{S}_{ijk}^{s,x}$$

we impose integral conservation over each stencil

$$\frac{1}{\Delta \mathbf{x}_e} \int_{x_{e-1/2}}^{x_{e+1/2}} \sum_{p=0}^M \psi_p(\xi(\mathbf{x})) \hat{\mathbf{w}}_{ijk,p}^{n,s} d\mathbf{x} = \bar{\mathbf{u}}_{ejk}^n, \quad \forall I_{ejk} \in \mathcal{S}_{ijk}^{s,x}$$

and perform a time-dependent nonlinear combination

$$\mathbf{w}_h^x(\mathbf{x}, t^n) = \sum_{p=0}^M \psi_p(\xi) \hat{\mathbf{w}}_{ijk,p}^n, \quad \text{with} \quad \hat{\mathbf{w}}_{ijk,p}^n = \sum_{s=1}^{N_s} \omega_s \hat{\mathbf{w}}_{ijk,p}^{n,s}$$

where

$$\omega_s = \frac{\tilde{\omega}_s}{\sum_k \tilde{\omega}_k}, \quad \tilde{\omega}_s = \frac{\lambda_s}{(\sigma_s + \epsilon)^r} \quad \epsilon = 10^{-4}, r = 3$$

$$\sigma_s = \sum_{p=1}^M \sum_{m=1}^M \Omega_{pm} \hat{\mathbf{w}}_{ijk,p}^{n,s} \hat{\mathbf{w}}_{ijk,m}^{n,s} \quad \Omega_{pm} = \sum_{\alpha=1}^M \int_0^1 \frac{\partial^\alpha \psi_p(\xi)}{\partial \xi^\alpha} \cdot \frac{\partial^\alpha \psi_m(\xi)}{\partial \xi^\alpha} d\xi$$

2) WENO reconstruction in **y direction** using as input the $M+1$ degrees of freedom $\hat{\mathbf{w}}_{ijk,p}^n$

$$\mathbf{w}_h^{s,y}(x, t^n) = \sum_{q=0}^M \sum_{p=0}^M \psi_p(\xi) \psi_q(\eta) \hat{\mathbf{w}}_{ijk,pq}^{n,s}$$

we now apply integral conservation in **y direction**.

$$\frac{1}{\Delta y_e} \int_{y_{e-1/2}}^{y_{e+1/2}} \sum_{q=0}^M \psi_q(\eta(y)) \hat{\mathbf{w}}_{ijk,pq}^{n,s} dy = \hat{\mathbf{w}}_{iek,p}^n, \quad \forall l_{iek} \in \mathcal{S}_{ijk}^{s,y}$$

and perform a time-dependent nonlinear combination

$$\mathbf{w}_h^y(x, y, t^n) = \sum_{q=0}^M \sum_{p=0}^M \psi_p(\xi) \psi_q(\eta) \hat{\mathbf{w}}_{ijk,pq}^n \quad \text{with} \quad \hat{\mathbf{w}}_{ijk,pq}^n = \sum_{s=1}^{N_s} \omega_s \hat{\mathbf{w}}_{ijk,pq}^{n,s}$$

2) WENO reconstruction in **z direction** using as input the $M+1$ degrees of freedom $\hat{\mathbf{w}}_{ijk,pq}^n$

$$\mathbf{w}_h^{s,y}(x, t^n) = \sum_{p=0}^M \sum_{q=0}^M \sum_{r=0}^M \psi_p(\xi) \psi_q(\eta) \psi_r(\zeta) \hat{\mathbf{w}}_{ijk,pqr}^{n,s}$$

we now apply integral conservation in **z direction**.

$$\frac{1}{\Delta z_e} \int_{z_{e-1/2}}^{z_{e+1/2}} \sum_{r=0}^M \psi_r(\zeta(z)) \hat{\mathbf{w}}_{ijk,pqr}^{n,s} dz = \hat{\mathbf{w}}_{ijk,pq}^n, \quad \forall l_{ije} \in \mathcal{S}_{ijk}^{s,z}$$

and perform a time-dependent nonlinear combination

$$\mathbf{w}_h^z(x, y, z, t^n) = \sum_{p=0}^M \sum_{q=0}^M \sum_{r=0}^M \psi_p(\xi) \psi_q(\eta) \psi_r(\zeta) \hat{\mathbf{w}}_{ijk,pqr}^n \quad \text{with} \quad \hat{\mathbf{w}}_{ijk,pqr}^n = \sum_{s=1}^{N_s} \omega_s \hat{\mathbf{w}}_{ijk,pqr}^{n,s}$$

References of this type of WENO reconstruction (just a few...)

Michael Dumbser, Martin Käser (2007). *Arbitrary high order non-oscillatory finite volume schemes on unstructured meshes for linear hyperbolic systems*. JCP 221 (2) pp 693-723.

Michael Dumbser, Dinshaw S. Balsara, Eleuterio F. Toro, Claus-Dieter Munz (2008). *A unified framework for the construction of one-step finite volume and discontinuous Galerkin schemes on unstructured meshes*. JCP 227 (18) pp 8209-8253.

Michael Dumbser, Cedric Enaux, Eleuterio F. Toro (2008). *Finite volume schemes of very high order of accuracy for stiff hyperbolic balance laws*. JCP 227 (8) pp 3971-4001.

Michael Dumbser, Manuel Castro, Carlos Parés, Eleuterio F. Toro (2009). *ADER schemes on unstructured meshes for nonconservative hyperbolic systems: Applications to geophysical flows*. C&F 38 (9) pp 1731-1748.

Michael Dumbser, Arturo Hidalgo, Manuel Castro, Carlos Parés, Eleuterio F. Toro (2010). *FORCE schemes on unstructured meshes II: Non-conservative hyperbolic systems*. CMAME 199 (9-12) pp 625-647.

Michael Dumbser, Arturo Hidalgo, Olindo Zanotti (2014). *High order space–time adaptive ADER-WENO finite volume schemes for non-conservative hyperbolic systems*. CMAME 268 (1) pp 359-387.

LOCAL SPACE TIME DG PREDICTOR

We write the equation in reference coordinates.

$$\frac{\partial \mathbf{u}}{\partial \tau} + \frac{\partial \mathbf{f}^*}{\partial \xi} + \frac{\partial \mathbf{g}^*}{\partial \eta} + \frac{\partial \mathbf{h}^*}{\partial \zeta} = \mathbf{S}^*$$

with:

$$\mathbf{f}^* = \frac{\Delta t}{\Delta x_i} \mathbf{f}, \quad \mathbf{g}^* = \frac{\Delta t}{\Delta y_j} \mathbf{g}, \quad \mathbf{h}^* = \frac{\Delta t}{\Delta z_k} \mathbf{h}, \quad \mathbf{S}^* = \Delta t \mathbf{S}$$

Now, we multiply by test functions and integrate in $[0,1]^4$:

$$\int_0^1 \int_0^1 \int_0^1 \int_0^1 \theta_q \left(\frac{\partial \mathbf{u}}{\partial \tau} + \frac{\partial \mathbf{f}^*}{\partial \xi} + \frac{\partial \mathbf{g}^*}{\partial \eta} + \frac{\partial \mathbf{h}^*}{\partial \zeta} - \mathbf{S}^* \right) d\xi d\eta d\zeta d\tau = 0$$

$$\theta_q(\xi, \eta, \zeta, \tau) = \psi_p(\xi) \psi_q(\eta) \psi_r(\zeta) \psi_s(\tau)$$

Integration by parts in time yields:

$$\int_0^1 \int_0^1 \int_0^1 \theta_q(\boldsymbol{\xi}, 1) \mathbf{u}(\boldsymbol{\xi}, 1) d\xi d\eta d\zeta - \int_0^1 \int_0^1 \int_0^1 \left(\frac{\partial}{\partial \tau} \theta_q \right) \mathbf{u} d\xi d\eta d\zeta d\tau$$
$$+ \int_0^1 \int_0^1 \int_0^1 \left[\theta_q \left(\frac{\partial \mathbf{f}^*}{\partial \xi} + \frac{\partial \mathbf{g}^*}{\partial \eta} + \frac{\partial \mathbf{h}^*}{\partial \zeta} - \mathbf{s}^* \right) \right] d\xi d\eta d\zeta d\tau =$$
$$= \int_0^1 \int_0^1 \int_0^1 \theta_q(\boldsymbol{\xi}, 0) \mathbf{w}_h(\boldsymbol{\xi}, t^n) d\xi d\eta d\zeta$$

$$\int_0^1 \int_0^1 \int_0^1 \int_0^1 \Theta_q \left(\frac{\partial \mathbf{u}}{\partial \tau} + \frac{\partial \mathbf{f}^*}{\partial \xi} + \frac{\partial \mathbf{g}^*}{\partial \eta} + \frac{\partial \mathbf{h}^*}{\partial \zeta} - \mathbf{S}^* \right) d\xi d\eta d\zeta d\tau = 0$$

Integration by parts in time yields:

$$\int_0^1 \int_0^1 \int_0^1 \theta_q(\xi, 1) \mathbf{u}(\xi, 1) d\xi d\eta d\zeta - \int_0^1 \int_0^1 \int_0^1 \int_0^1 \left(\frac{\partial}{\partial \tau} \theta_q \right) \mathbf{u} d\xi d\eta d\zeta d\tau$$

$$+ \int_0^1 \int_0^1 \int_0^1 \int_0^1 \left[\theta_q \left(\frac{\partial \mathbf{f}^*}{\partial \xi} + \frac{\partial \mathbf{g}^*}{\partial \eta} + \frac{\partial \mathbf{h}^*}{\partial \zeta} - \mathbf{s}^* \right) \right] d\xi d\eta d\zeta d\tau =$$

$$= \int_0^1 \int_0^1 \int_0^1 \theta_q(\xi, 0) \mathbf{w}_h(\xi, t^n) d\xi d\eta d\zeta$$



$$\int_0^1 \int_0^1 \int_0^1 \int_0^1 \theta_q \left(\frac{\partial \mathbf{u}}{\partial \tau} + \frac{\partial \mathbf{f}^*}{\partial \xi} + \frac{\partial \mathbf{g}^*}{\partial \eta} + \frac{\partial \mathbf{h}^*}{\partial \zeta} - \mathbf{s}^* \right) d\xi d\eta d\zeta d\tau = 0$$

we denote the discrete space-time solution by \mathbf{q}_h for which we make the following ansatz.

$$\mathbf{q}_h = \mathbf{q}_h(\xi) = \theta_p(\xi, \tau) \hat{\mathbf{q}}_p$$

With the yet unknown degrees of freedom $\hat{\mathbf{q}}_p = \hat{\mathbf{q}}_{pqrs}$

we use the same representation for the fluxes and source term

$$\mathbf{f}_h^* = \theta_p \hat{\mathbf{f}}_p^*, \quad \mathbf{g}_h^* = \theta_p \hat{\mathbf{g}}_p^*, \quad \mathbf{h}_h^* = \theta_p \hat{\mathbf{h}}_p^*, \quad \mathbf{s}_h^* = \theta_p \hat{\mathbf{s}}_p^*.$$

Due to the nodal approach, the above degrees of freedom for the fluxes and source terms are simply the point-wise evaluation of the physical fluxes and source terms, hence

$$\hat{\mathbf{f}}_p^* = \mathbf{f}^*(\hat{\mathbf{q}}_p), \quad \hat{\mathbf{g}}_p^* = \mathbf{g}^*(\hat{\mathbf{q}}_p), \quad \hat{\mathbf{h}}_p^* = \mathbf{h}^*(\hat{\mathbf{q}}_p), \quad \hat{\mathbf{s}}_p^* = \mathbf{s}^*(\hat{\mathbf{q}}_p)$$

$$\begin{aligned}
& \int_0^1 \int_0^1 \int_0^1 \theta_q(\boldsymbol{\xi}, 1) \theta_p(\boldsymbol{\xi}, 1) \hat{\mathbf{q}}_p \, d\xi d\eta d\zeta - \int_0^1 \int_0^1 \int_0^1 \int_0^1 \left(\frac{\partial}{\partial \tau} \theta_q \right) \theta_p \hat{\mathbf{q}}_p \, d\xi d\eta d\zeta d\tau \\
& + \int_0^1 \int_0^1 \int_0^1 \int_0^1 \left[\theta_q \left(\frac{\partial}{\partial \xi} \theta_p \hat{\mathbf{f}}_p^* + \frac{\partial}{\partial \eta} \theta_p \hat{\mathbf{g}}_p^* + \frac{\partial}{\partial \zeta} \theta_p \hat{\mathbf{h}}_p^* - \theta_p \hat{\mathbf{s}}_p^* \right) \right] d\xi d\eta d\zeta d\tau \\
& = \int_0^1 \int_0^1 \int_0^1 \theta_q(\boldsymbol{\xi}, 0) \hat{\mathbf{w}}_h(\boldsymbol{\xi}, t^n) d\xi d\eta d\zeta
\end{aligned}$$

which is weak form is an element-local nonlinear algebraic equation system for the unknown coefficients $\hat{\mathbf{q}}_p$. The initial condition is included in a weak sense by the integral on the right hand side, where the reconstructed solution $\hat{\mathbf{w}}_h(\boldsymbol{\xi}, t^n)$

After introducing the integrals

$$\mathbf{K}_{qp}^1 = \int_0^1 \int_0^1 \int_0^1 \theta_q(\boldsymbol{\xi}, 1) \theta_p(\boldsymbol{\xi}, 1) d\boldsymbol{\xi} - \int_0^1 \int_0^1 \int_0^1 \int_0^1 \left(\frac{\partial}{\partial \tau} \theta_q \right) \theta_p d\boldsymbol{\xi} d\tau$$

$$\mathbf{K}_{qp}^\xi = (\mathbf{K}_{qp}^\xi, \mathbf{K}_{qp}^\eta, \mathbf{K}_{qp}^\zeta) = \int_0^1 \int_0^1 \int_0^1 \int_0^1 \theta_q \frac{\partial}{\partial \xi} \theta_p d\xi d\tau \quad \mathbf{M}_{qp} = \int_0^1 \int_0^1 \int_0^1 \int_0^1 \theta_q \theta_p d\boldsymbol{\xi} d\tau$$

$$\mathbf{F}_{qp}^0 = \int_0^1 \int_0^1 \int_0^1 \theta_q(\boldsymbol{\xi}, 0) \psi_m(\boldsymbol{\xi}) d\boldsymbol{\xi}$$

where $d\boldsymbol{\xi} = d\xi d\eta d\zeta$ one can rewrite the above system in compact matrix-vector form as

$$\mathbf{K}_{qp}^1 \hat{\mathbf{q}}_p + \mathbf{K}_{qp}^\xi \cdot \hat{\mathbf{f}}_p^* + \mathbf{K}_{qp}^\eta \hat{\mathbf{g}}_p^* + \mathbf{K}_{qp}^\zeta \hat{\mathbf{h}}_p^* = \mathbf{M}_{qp} \hat{\mathbf{S}}_p^* + \mathbf{F}_{qm}^0 \hat{\mathbf{w}}_m^n$$

with the spatial multi-index $m = (k, l, m)$ and $\psi_m(\boldsymbol{\xi}) = \psi_k(\xi) \psi_l(\eta) \psi_m(\zeta)$

The system is conveniently solved by the following iterative scheme, introduced in Dumbser & Zanotti (2008)

$$\mathbf{K}_{qp}^1 \hat{\mathbf{q}}_p^{k+1} - \mathbf{M}_{qp} \hat{\mathbf{S}}_p^{*,k+1} = \mathbf{F}_{qm}^0 \hat{\mathbf{w}}_m^n - \mathbf{K}_{qp}^\xi \hat{\mathbf{f}}_p^{*,k} - \mathbf{K}_{qp}^\eta \hat{\mathbf{g}}_p^{*,k} - \mathbf{K}_{qp}^\zeta \hat{\mathbf{h}}_p^{*,k}$$

Also, an efficient second-order MUSCLE-type initial guess has been proposed in Hidalgo & Dumbser (2010)

$$\mathbf{K}_{qp}^1 \hat{\mathbf{q}}_p^{k+1} - \mathbf{M}_{qp} \hat{\mathbf{S}}_p^{*,k+1} = \mathbf{F}_{qm}^0 \hat{\mathbf{w}}_m^n - \mathbf{K}_{qp}^\xi \hat{\mathbf{f}}_p^{*,k} - \mathbf{K}_{qp}^\eta \hat{\mathbf{g}}_p^{*,k} - \mathbf{K}_{qp}^\zeta \hat{\mathbf{h}}_p^{*,k}$$

then we can write the scheme as

$$\begin{aligned} \mathbf{u}_{ijk}^{n+1} = \mathbf{u}_{ijk}^n &+ \frac{\Delta t}{\Delta x_i} (\mathbf{f}_{i+1/2,j,k} - \mathbf{f}_{i-1/2,j,k}) + \frac{\Delta t}{\Delta y_j} (\mathbf{g}_{i,j+1/2,k} - \mathbf{g}_{i,j-1/2,k}) + \\ &+ \frac{\Delta t}{\Delta z_k} (\mathbf{h}_{i,j,k+1/2} - \mathbf{h}_{i,j,k-1/2}) = \Delta t \mathbf{S}_{ijk} \end{aligned}$$

$$\mathbf{K}_{qp}^1 \hat{\mathbf{q}}_p^{k+1} - \mathbf{M}_{qp} \hat{\mathbf{S}}_p^{*,k+1} = \mathbf{F}_{qm}^0 \hat{\mathbf{w}}_m^n - \mathbf{K}_{qp}^\xi \hat{\mathbf{f}}_p^{*,k} - \mathbf{K}_{qp}^\eta \hat{\mathbf{g}}_p^{*,k} - \mathbf{K}_{qp}^\zeta \hat{\mathbf{h}}_p^{*,k}$$

then we can write the scheme as

$$\begin{aligned} \mathbf{u}_{ijk}^{n+1} = \mathbf{u}_{ijk}^n + \frac{\Delta t}{\Delta x_i} (\mathbf{f}_{i+1/2,j,k} - \mathbf{f}_{i-1/2,j,k}) + \frac{\Delta t}{\Delta y_j} (\mathbf{g}_{i,j+1/2,k} - \mathbf{g}_{i,j-1/2,k}) + \\ + \frac{\Delta t}{\Delta z_k} (\mathbf{h}_{i,j,k+1/2} - \mathbf{h}_{i,j,k-1/2}) = \Delta t \mathbf{S}_{ijk} \end{aligned}$$

And use an appropriate numerical flux:

$$\tilde{\mathbf{f}}(\mathbf{q}_h^-, \mathbf{q}_h^+) = \frac{1}{2} (\mathbf{f}(\mathbf{q}_h^+) + \mathbf{f}(\mathbf{q}_h^-)) + \frac{1}{2} |\mathbf{S}_{\max}| (\mathbf{q}_h^+ - \mathbf{q}_h^-)$$

$$\tilde{\mathbf{f}}(\mathbf{q}_h^-, \mathbf{q}_h^+) = \frac{1}{2} (\mathbf{f}(\mathbf{q}_h^+) + \mathbf{f}(\mathbf{q}_h^-)) + \frac{1}{2} \left(\int_0^1 |\mathbf{A}(\psi(s))| ds \right) (\mathbf{q}_h^+ - \mathbf{q}_h^-)$$

This local space-time DG is a variant of ADER approach introduced to treat accurately stiff source terms. It also avoids the use of the rather cumbersome Cauchy-Kowalewski procedure of the original ADER.

Michael Dumbser, Cedric Enaux, Eleuterio F. Toro (2008). *Finite volume schemes of very high order of accuracy for stiff hyperbolic balance laws*. JCP 227 (8) pp 3971-4001.

ADAPTIVE MESH REFINEMENT

We have developed a cell-by-cell AMR technique in which the computational domain is discretized with a uniform Cartesian grid at the coarsest level.

We adopt a refinement criterion marking a cell for refinement if

$$\chi_m > \chi_{\text{ref}}$$

where

$$\chi_m = \sqrt{\frac{\sum_{k,l} (\partial^2 \Phi / \partial x_k \partial x_l)^2}{\sum_{k,l} [(|\partial \Phi / \partial x_k|_{i+1} + |\partial \Phi / \partial x_k|_i) / \Delta x_l + \varepsilon] (\partial^2 / \partial x_k \partial x_l) \|\Phi\|^2}}.$$

When a cell of the level ℓ is refined, it is subdivided into an integer number \mathfrak{r} of finer cells along each direction, such that

$$\Delta x_{\ell} = \mathfrak{r} \Delta x_{\ell+1} \quad \Delta y_{\ell} = \mathfrak{r} \Delta y_{\ell+1} \quad \Delta z_{\ell} = \mathfrak{r} \Delta z_{\ell+1}$$

and also the time steps are chosen locally on each level so that

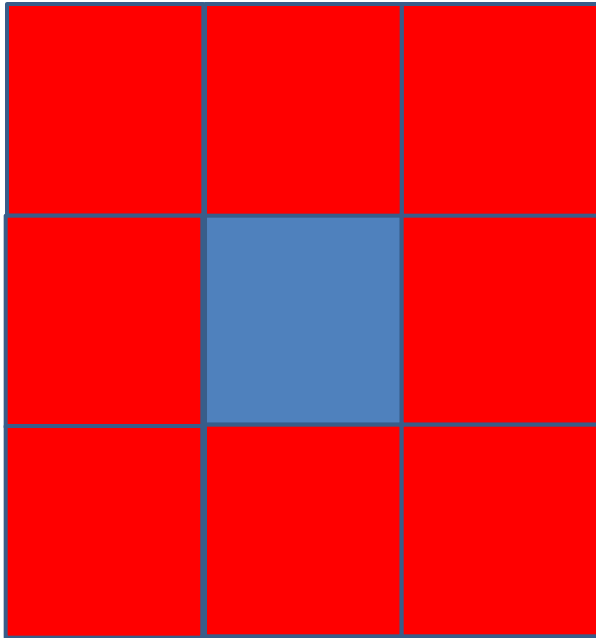
$$\Delta t_{\ell} = \mathfrak{r} \Delta t_{\ell+1}$$

As a result, each *mother* cell generates \mathfrak{r}^d *children* cells in d space dimensions.

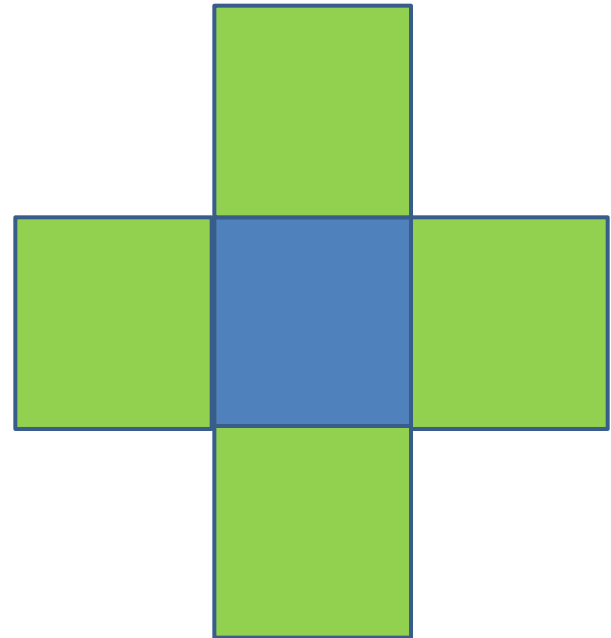
Possible status for a cell:

- Active regular cell.
- Virtual child cell.
- Virtual mother cell.

Voronoi neighbours: They share a node



Neumann neighbours: They share a face



Some rules...

If the Voronoi neighbours of an active refine cell C_m are not at the same level of refinement of cell C_m they have *virtual* children at the same level of refinement of cell C_m

In order to keep the reconstruction local on the coarser grid level we need $r \geq M$

The levels of refinement of two cells that are Voronoi neighbours of each other must differ on a unity, at most.

And one interesting property...

The local space-time DG predictor does not need exchange of information with neighbour elements, although they are in different levels of refinement.

Typical AMR operations

Projection:

An ACTIVE MOTHER assigns values to the VIRTUAL CHILDREN,

$$\bar{\mathbf{u}}_m(t_\ell^n) = \frac{1}{\Delta x_\ell} \frac{1}{\Delta y_\ell} \frac{1}{\Delta z_\ell} \int_{C_m} \mathbf{q}_h(\mathbf{x}, t_\ell^n) d\mathbf{x}$$

needed for performing the reconstruction on the finer grid level at intermediate times.

Typical AMR operations

Projection:

An ACTIVE MOTHER assigns values to the VIRTUAL CHILDREN,

$$\bar{\mathbf{u}}_m(t_\ell^n) = \frac{1}{\Delta x_\ell} \frac{1}{\Delta y_\ell} \frac{1}{\Delta z_\ell} \int_{C_m} \mathbf{q}_h(\mathbf{x}, t_\ell^n) d\mathbf{x}$$

needed for performing the reconstruction on the finer grid level at intermediate times.

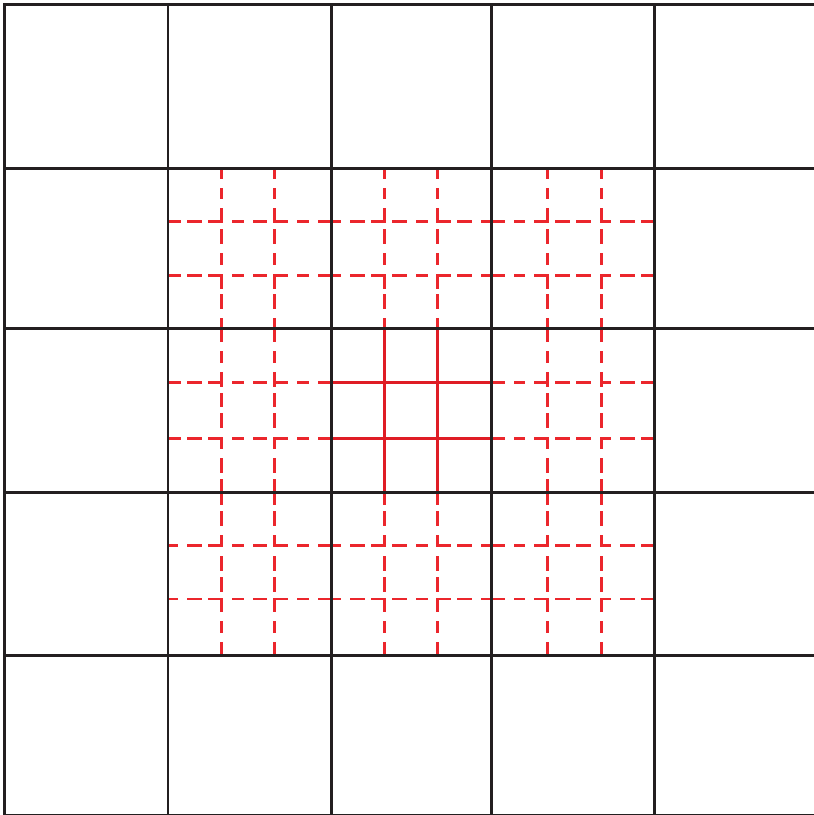
Averaging:

A VIRTUAL MOTHER obtains its average by averaging recursively over the cell averages of all its children at higher refinement levels,

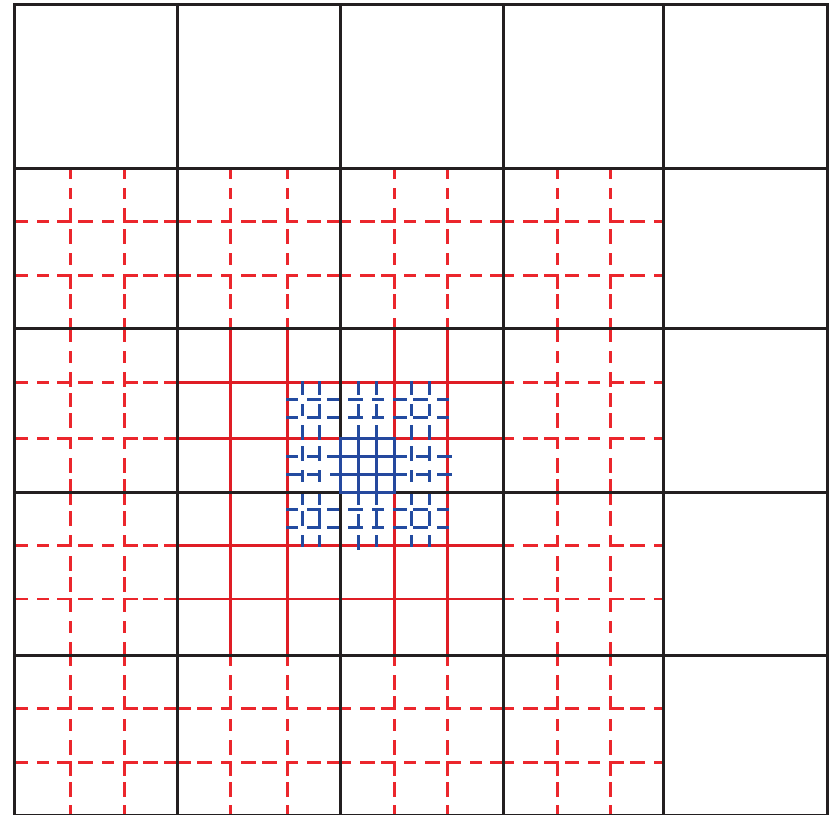
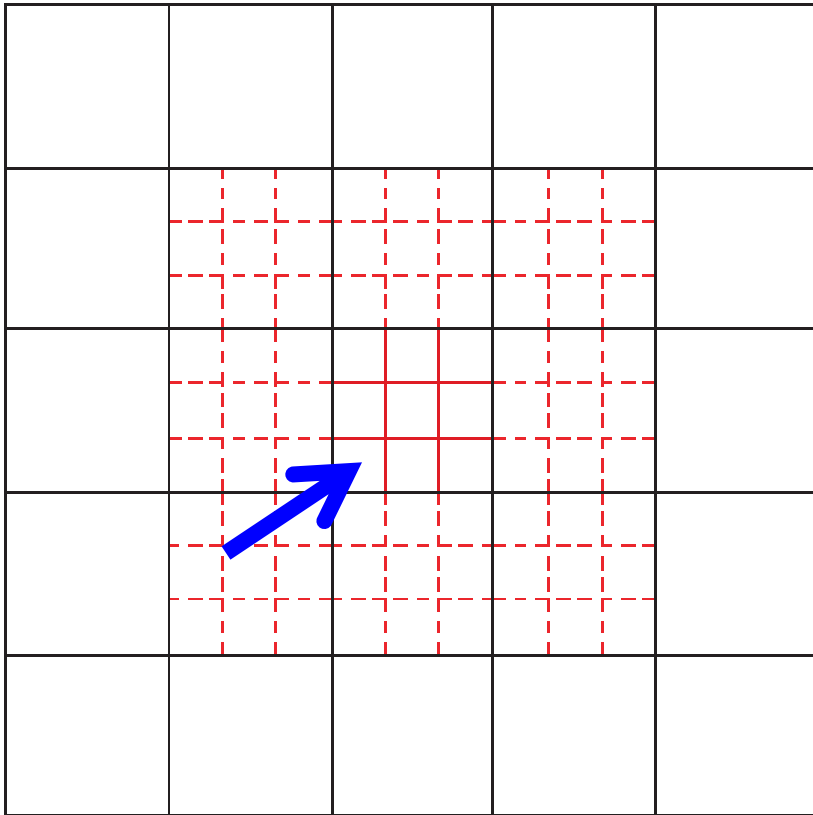
$$\bar{\mathbf{u}}_m = \frac{1}{r^d} \sum_{C_k \in \mathcal{B}_m} \bar{\mathbf{u}}_k$$

needed for performing the reconstruction on the finer grid level at intermediate times.

Refinement mechanism involving two levels of refinement ($k=2$) in a 2D geometry. Solid lines: active cells; dashed lines: virtual cells.



Refinement mechanism involving two levels of refinement ($k=2$) in a 2D geometry. Solid lines: active cells; dashed lines: virtual cells.



LOCAL TIME-STEPPING

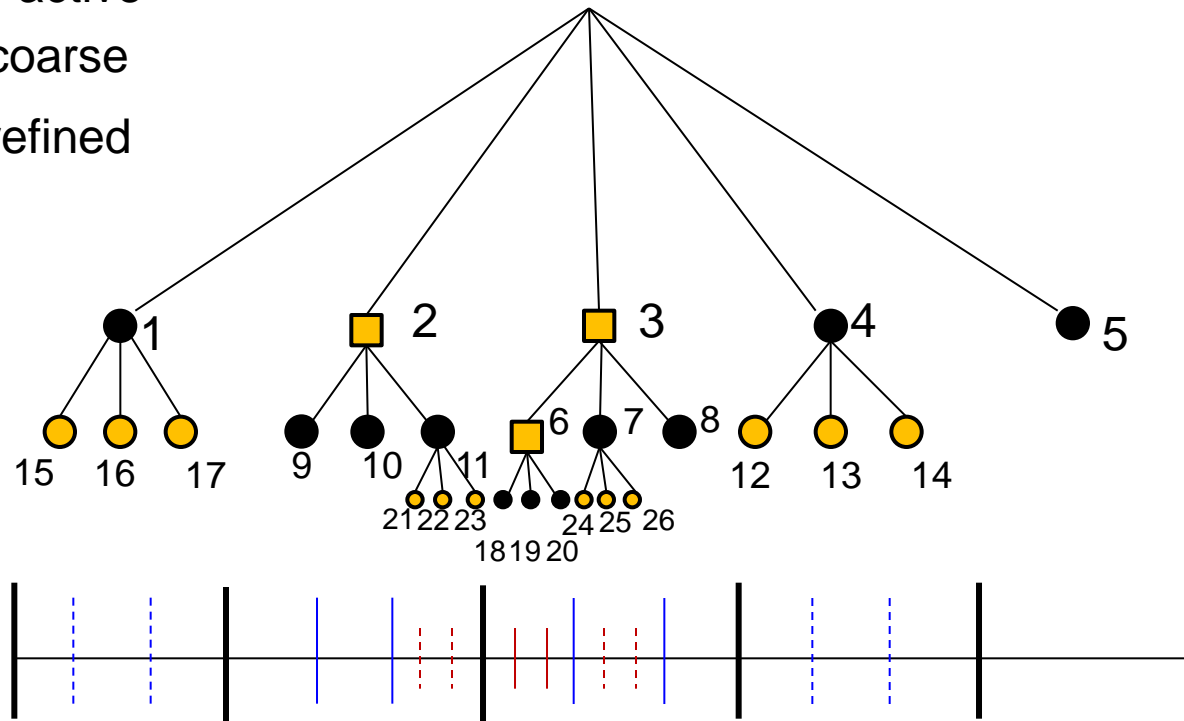
Each refinement level is advanced in time with its own *local* time step.

$$\Delta t_\ell = \tau \Delta t_{\ell+1}$$

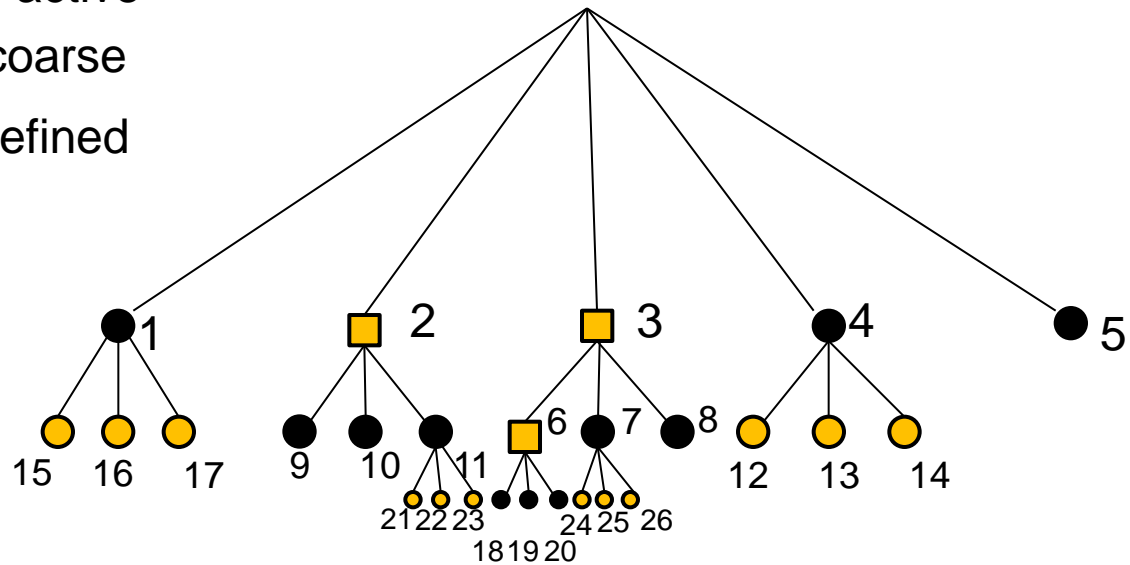
starting from the common initial time $t=0$, the finest level of refinement ℓ_{\max} is evolved first and performs a number of sub-time steps τ before the next coarser level $\ell_{\max} - 1$ performs its first time update.

This procedure is then applied recursively and it implies a total amount of τ^ℓ sub-time steps on each level to be performed in order to reach the time t_0^{n+1} of the coarsest level.

- Regular active
- Virtual coarse
- Virtual refined

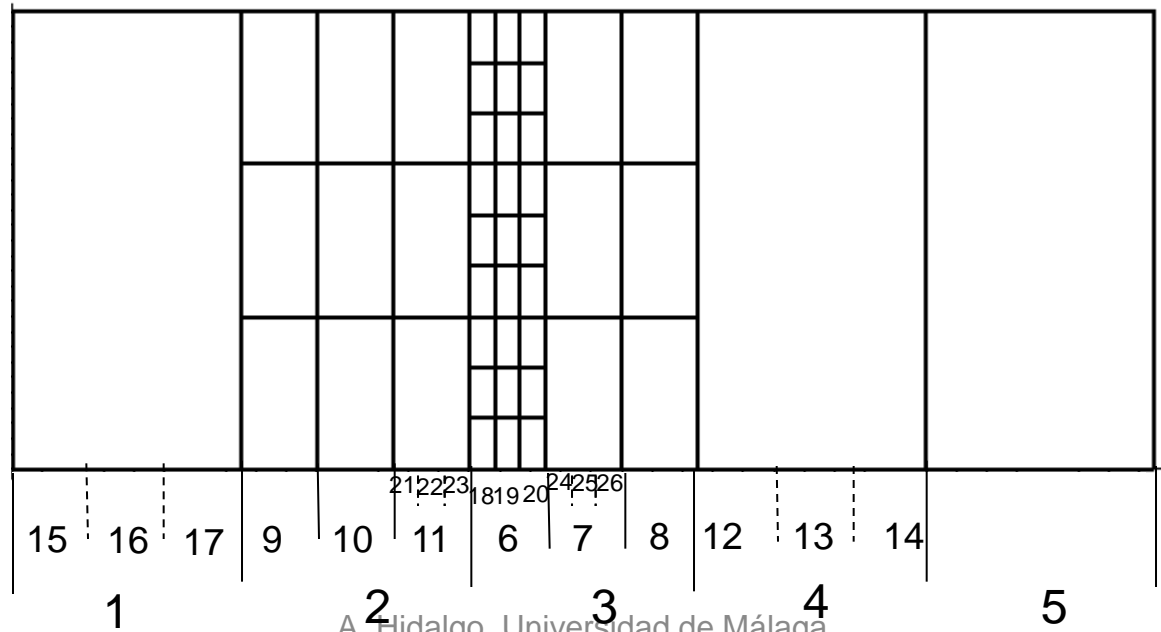


- Regular active
- Virtual coarse
- Virtual refined

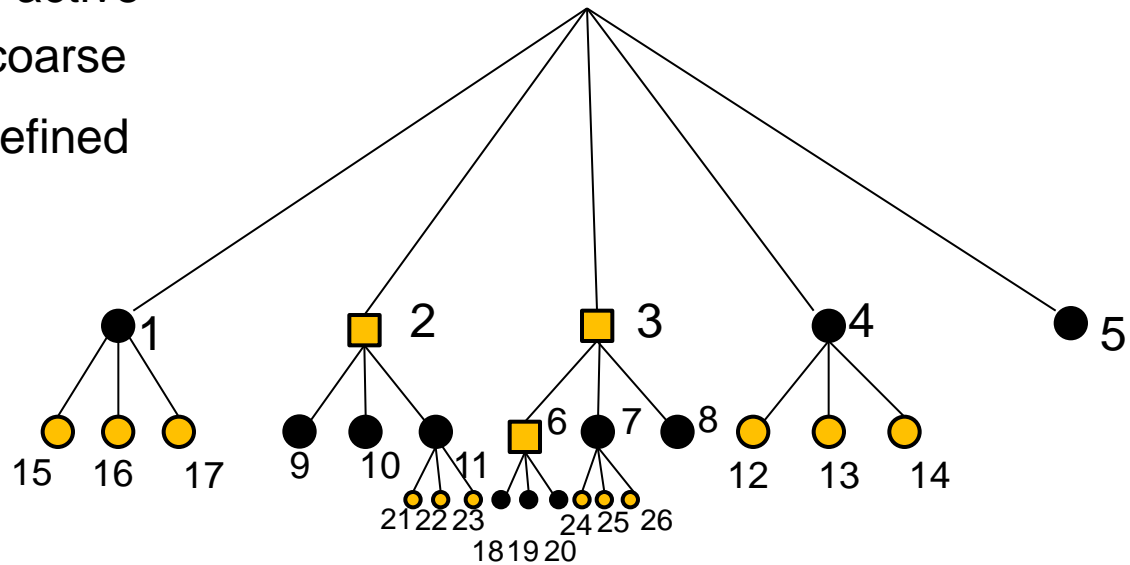


t^{n+1}

t^n

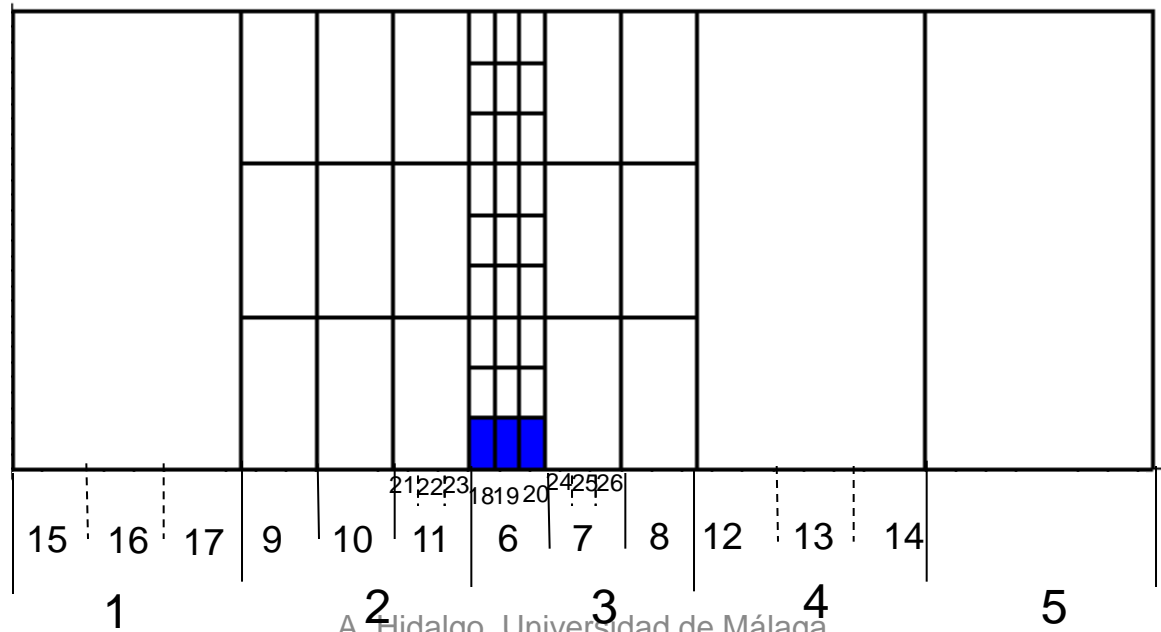


- Regular active
- Virtual coarse
- Virtual refined

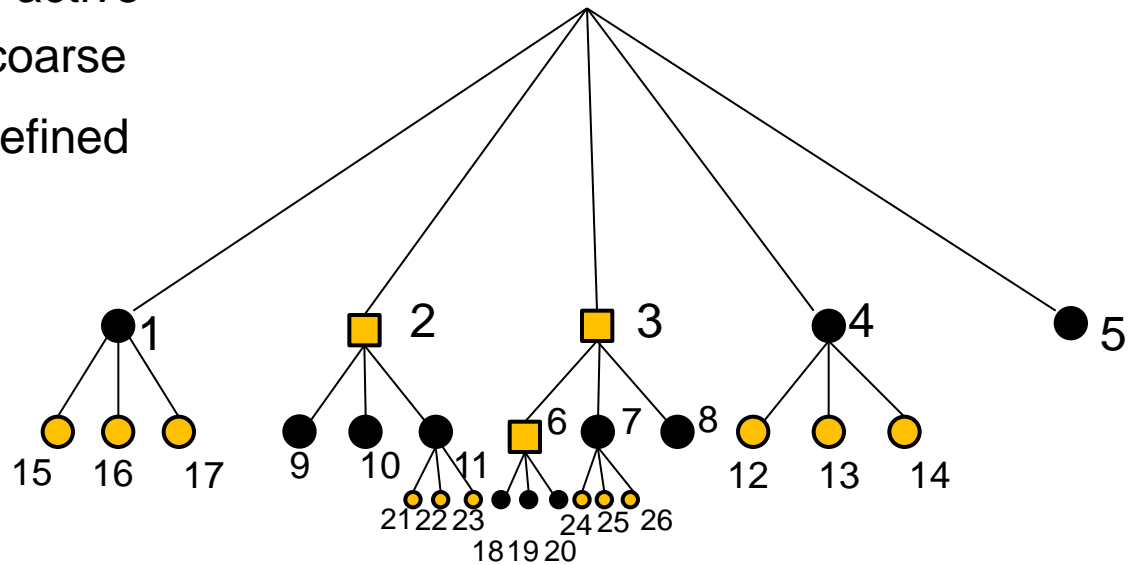


t^{n+1}

t^n

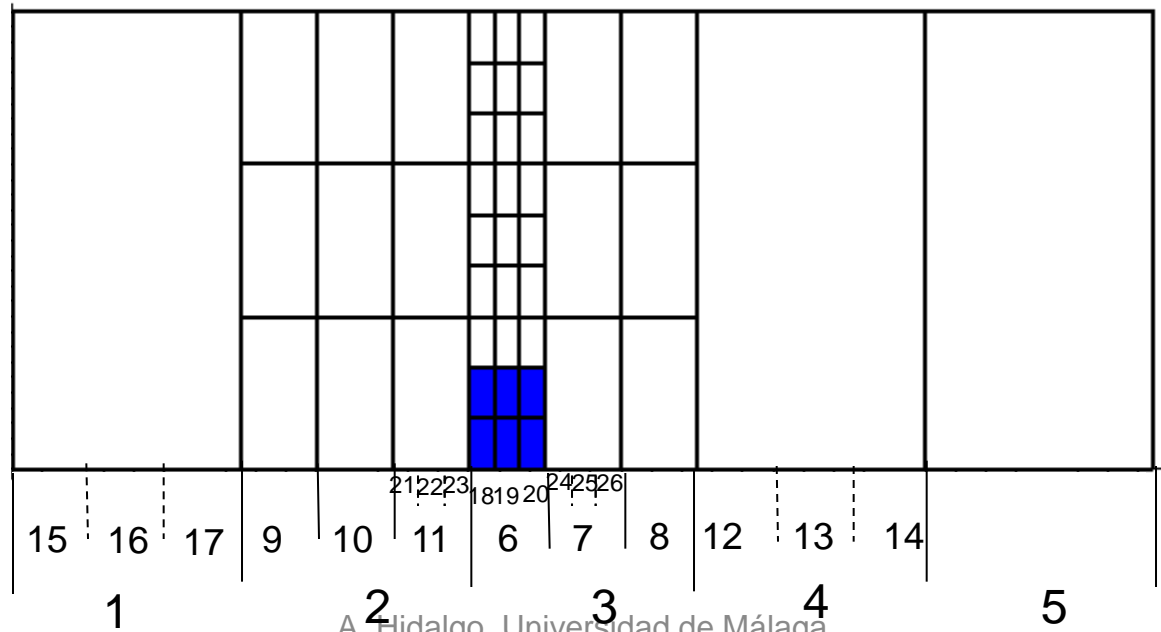


- Regular active
- Virtual coarse
- Virtual refined

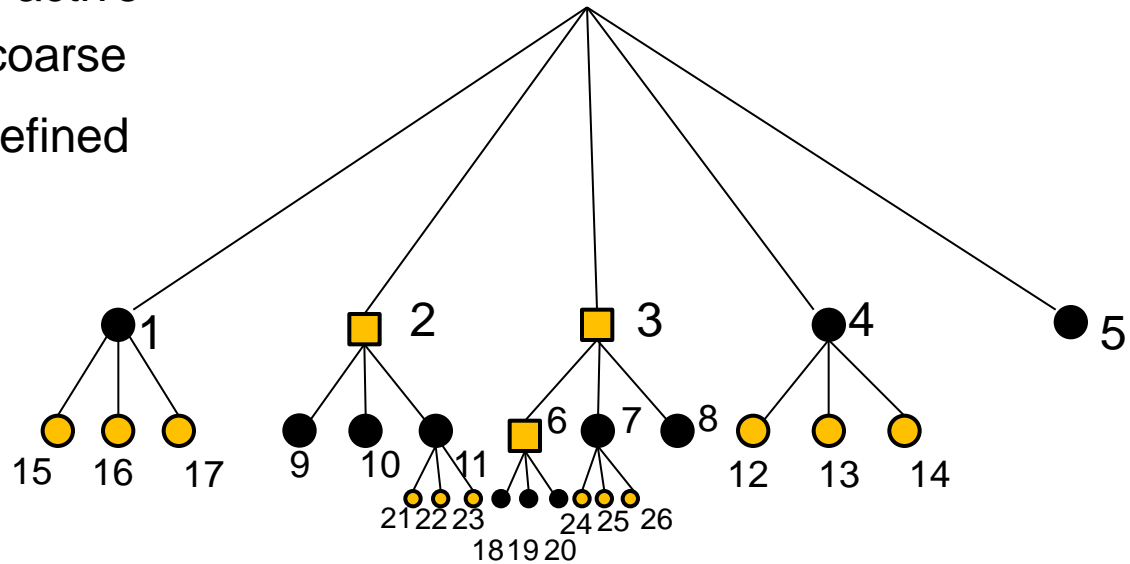


t^{n+1}

t^n

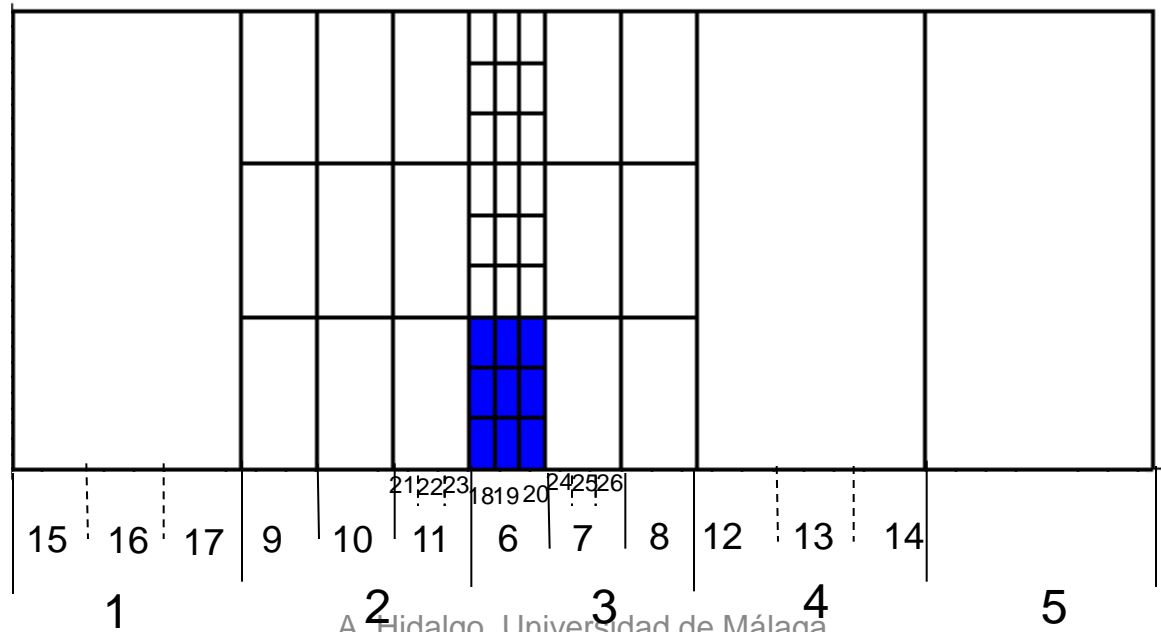


- Regular active
- Virtual coarse
- Virtual refined

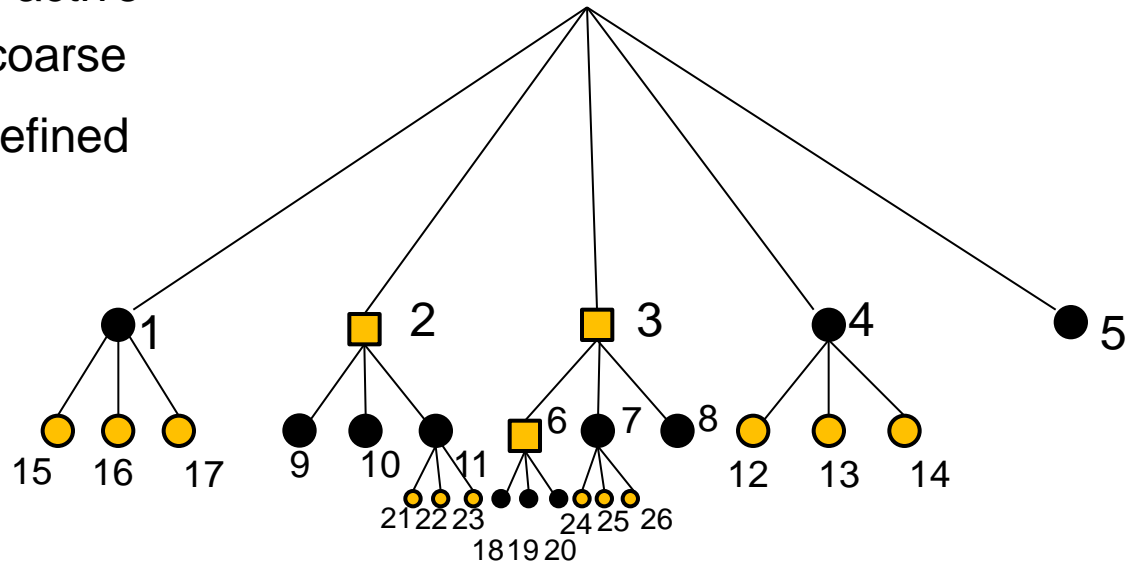


t^{n+1}

t^n

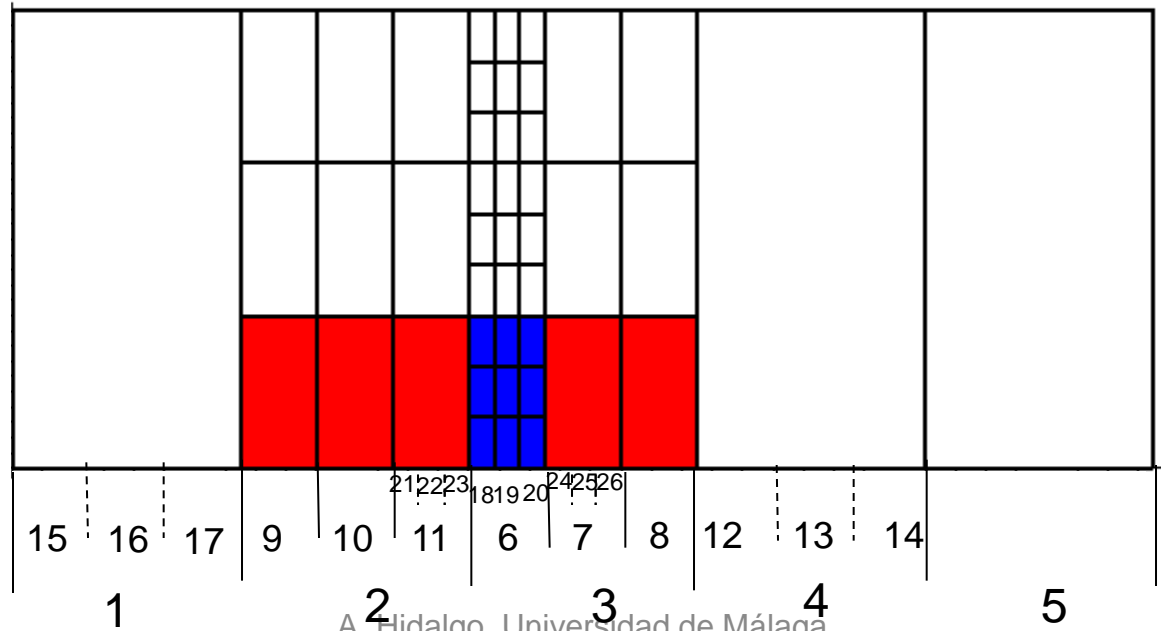


- Regular active
- Virtual coarse
- Virtual refined

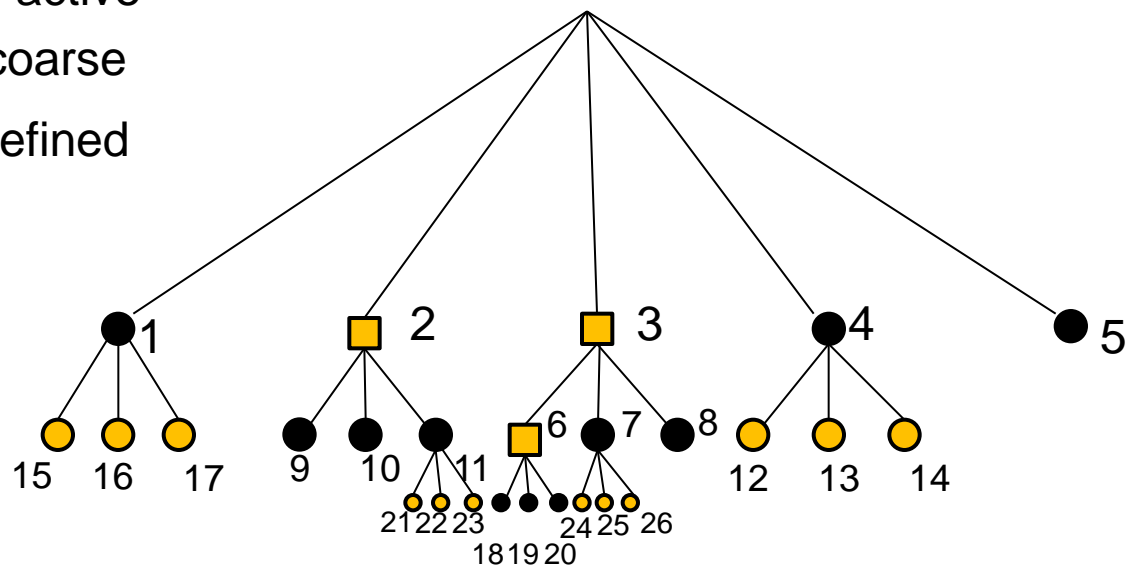


t^{n+1}

t^n

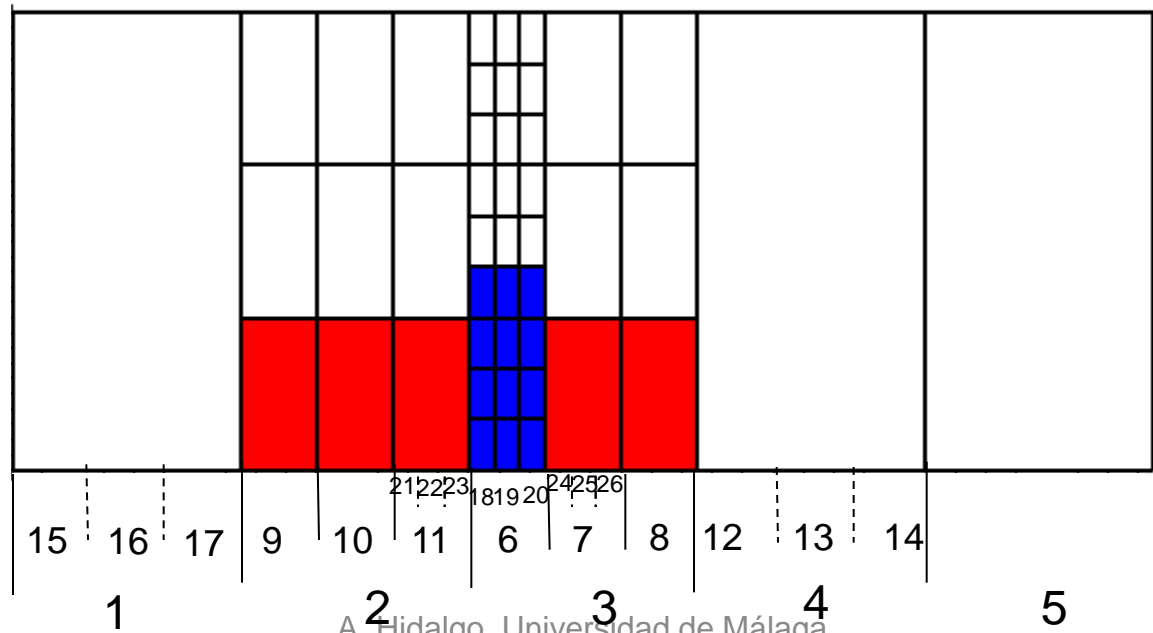


- Regular active
- Virtual coarse
- Virtual refined



t^{n+1}

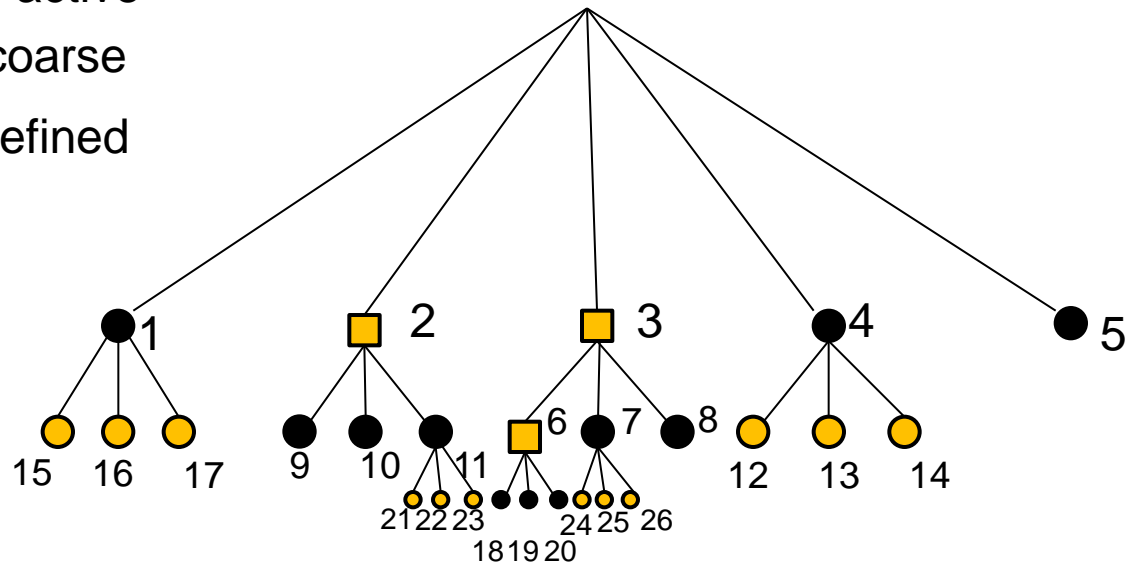
t^n



-
- Regular active
 ■ Virtual coarse
 ● Virtual refined
- The diagram shows a hierarchical tree structure. The root node is a black circle. It has five children: node 1 (black circle), node 2 (yellow square), node 3 (yellow square), node 4 (black circle), and node 5 (black circle). Node 1 has three children: node 15 (yellow circle), node 16 (yellow circle), and node 17 (yellow circle). Node 2 has three children: node 9 (black circle), node 10 (black circle), and node 11 (black circle). Node 3 has four children: node 6 (yellow square), node 7 (black circle), node 8 (black circle), and node 12 (yellow circle). Node 4 has three children: node 13 (yellow circle), node 14 (yellow circle), and node 18 (yellow circle). Node 5 has no children. Node 11 has three children: node 21 (yellow circle), node 22 (yellow circle), and node 23 (yellow circle). Node 6 has three children: node 18 (yellow circle), node 19 (yellow circle), and node 20 (yellow circle). Node 7 has three children: node 24 (yellow circle), node 25 (yellow circle), and node 26 (yellow circle).

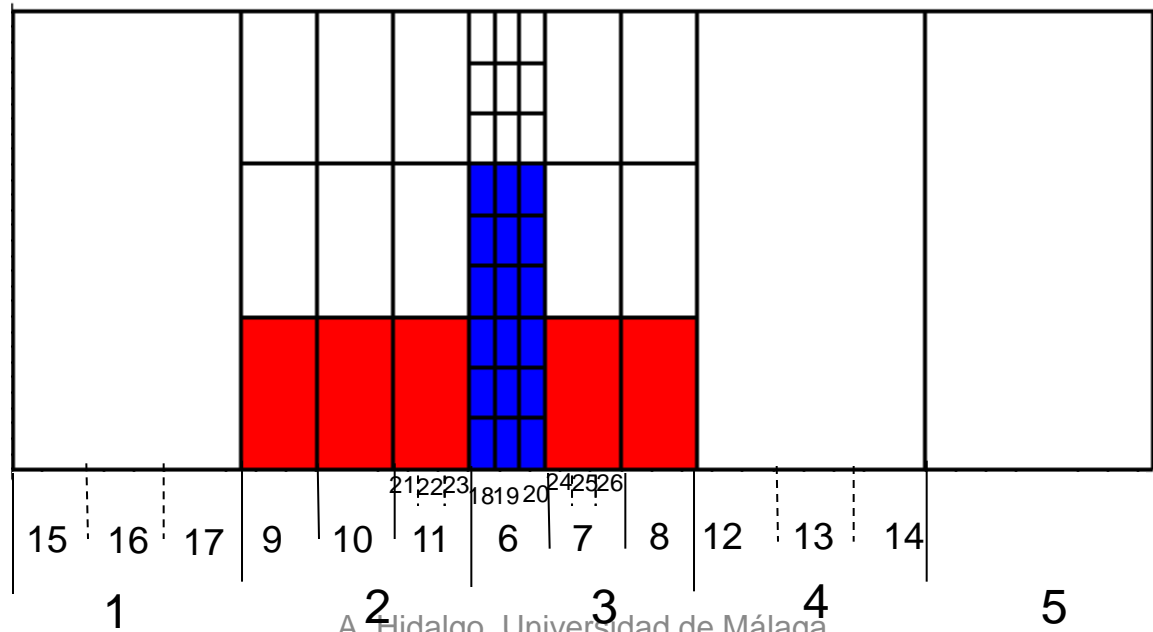


- Regular active
- Virtual coarse
- Virtual refined

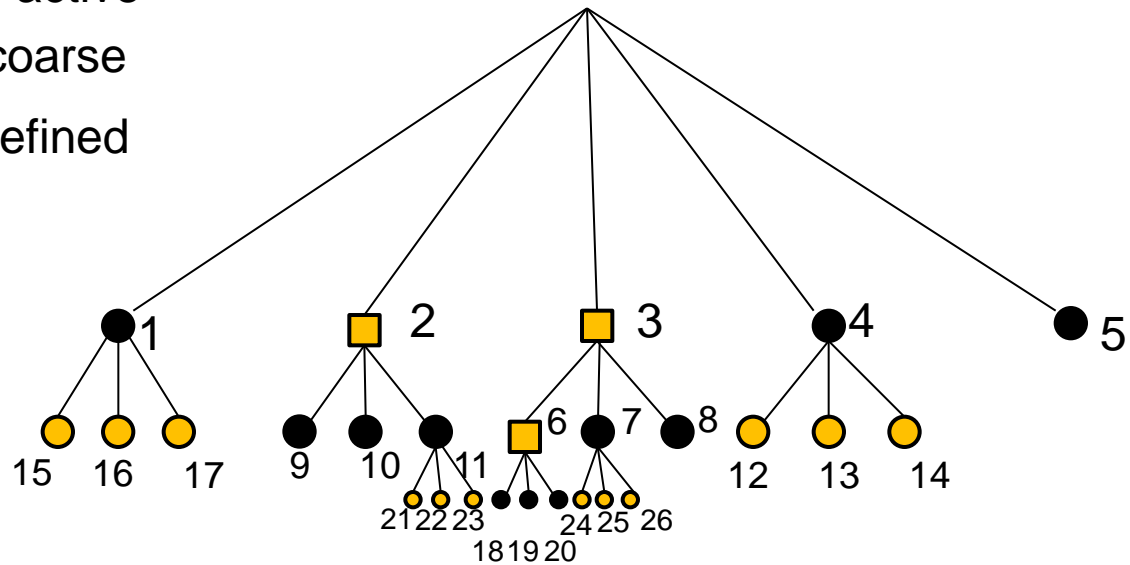


t^{n+1}

t^n

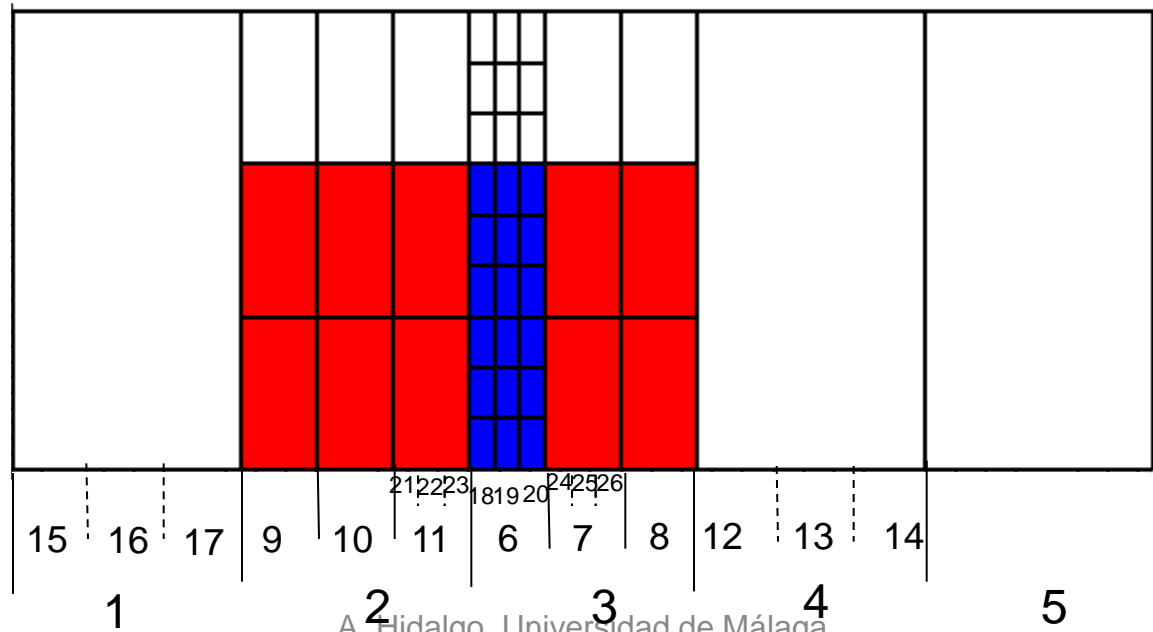


- Regular active
- Virtual coarse
- Virtual refined

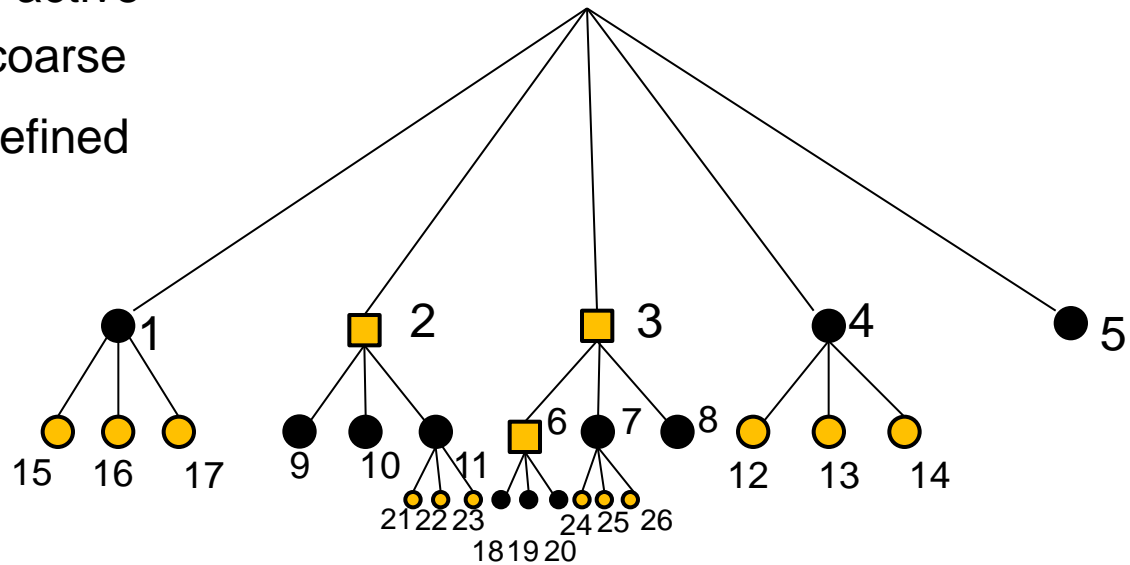


t^{n+1}

t^n

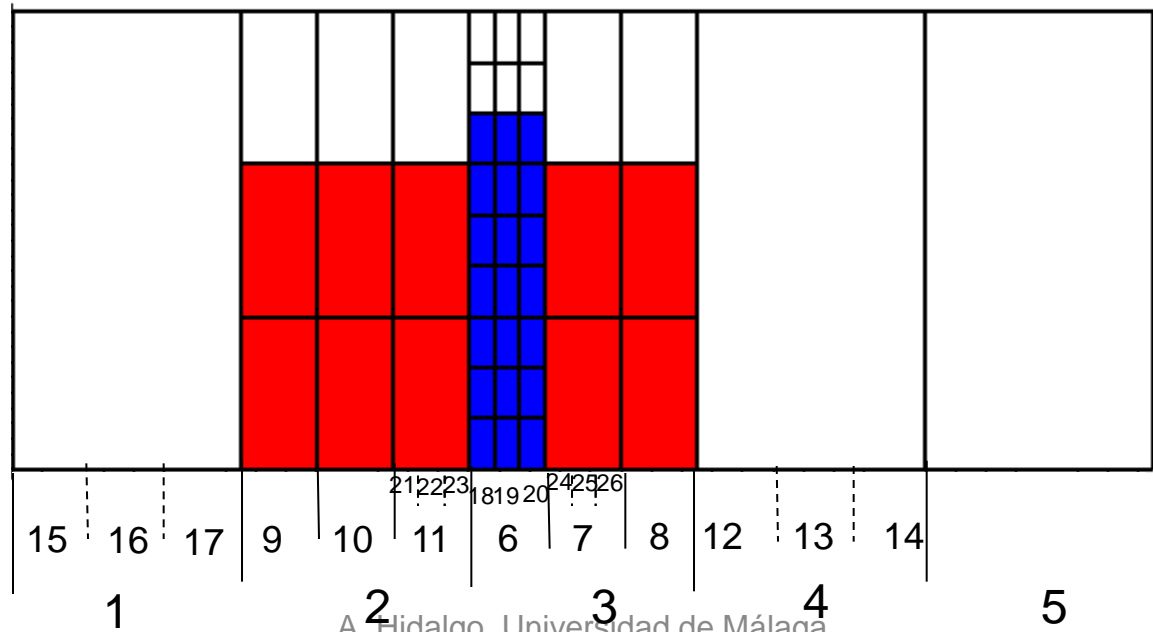


- Regular active
- Virtual coarse
- Virtual refined

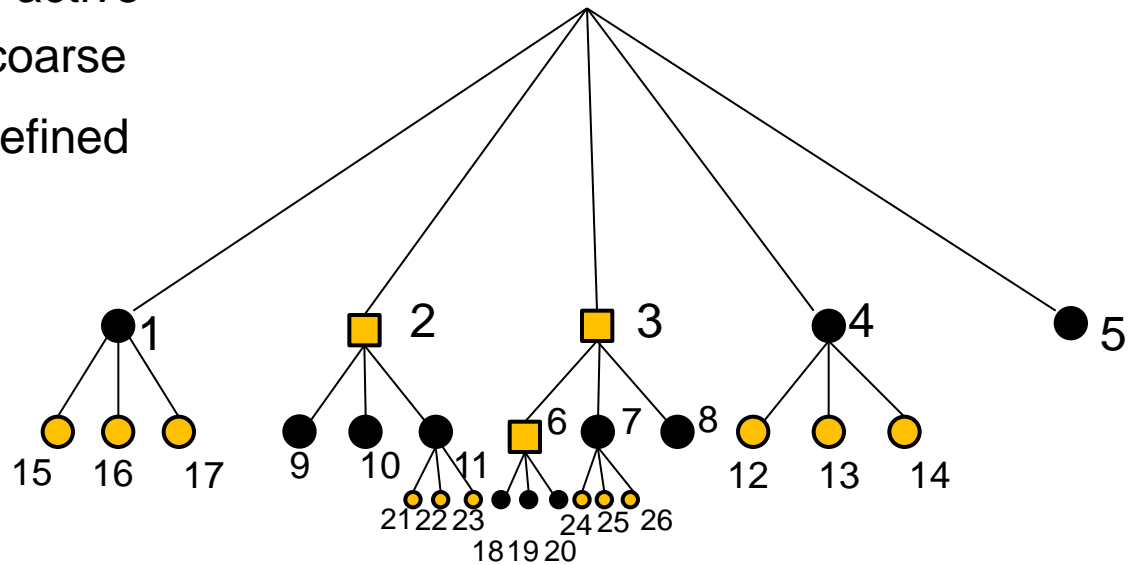


t^{n+1}

t^n

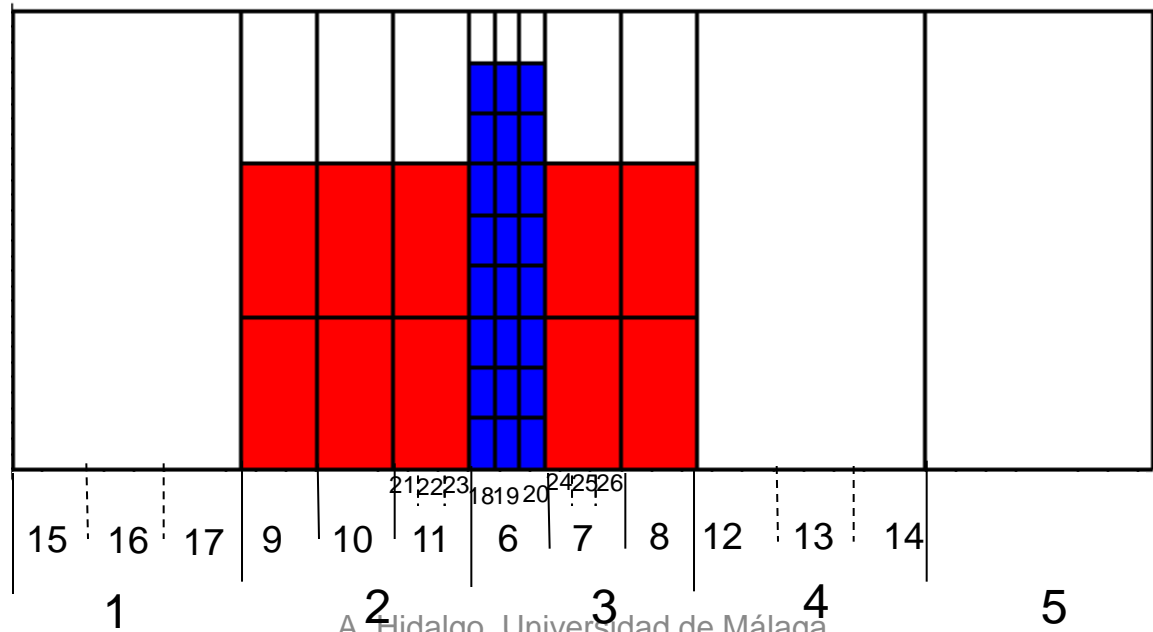


- Regular active
- Virtual coarse
- Virtual refined

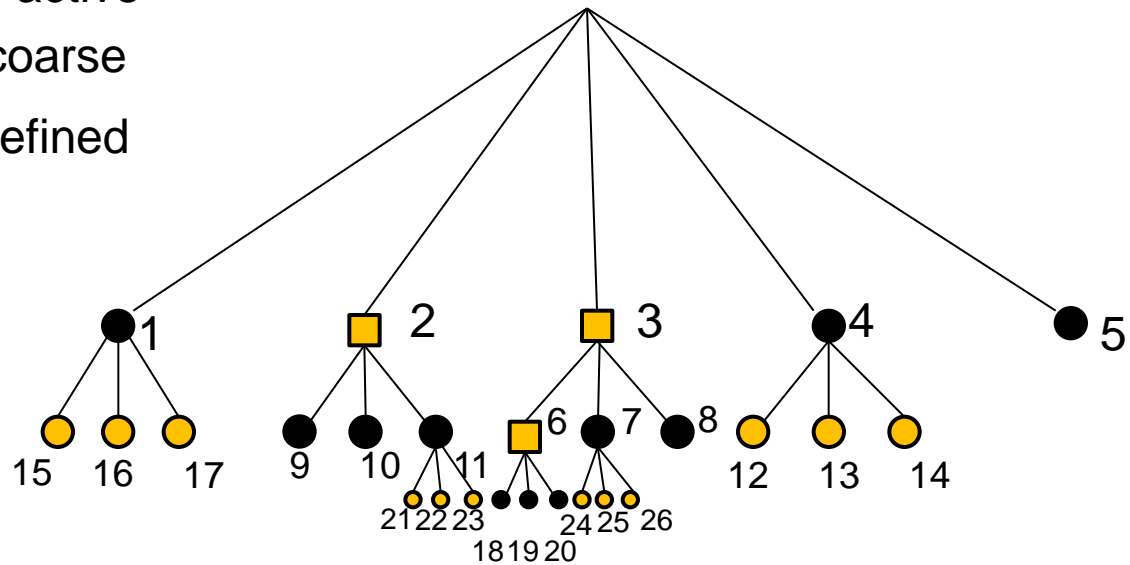


t^{n+1}

t^n

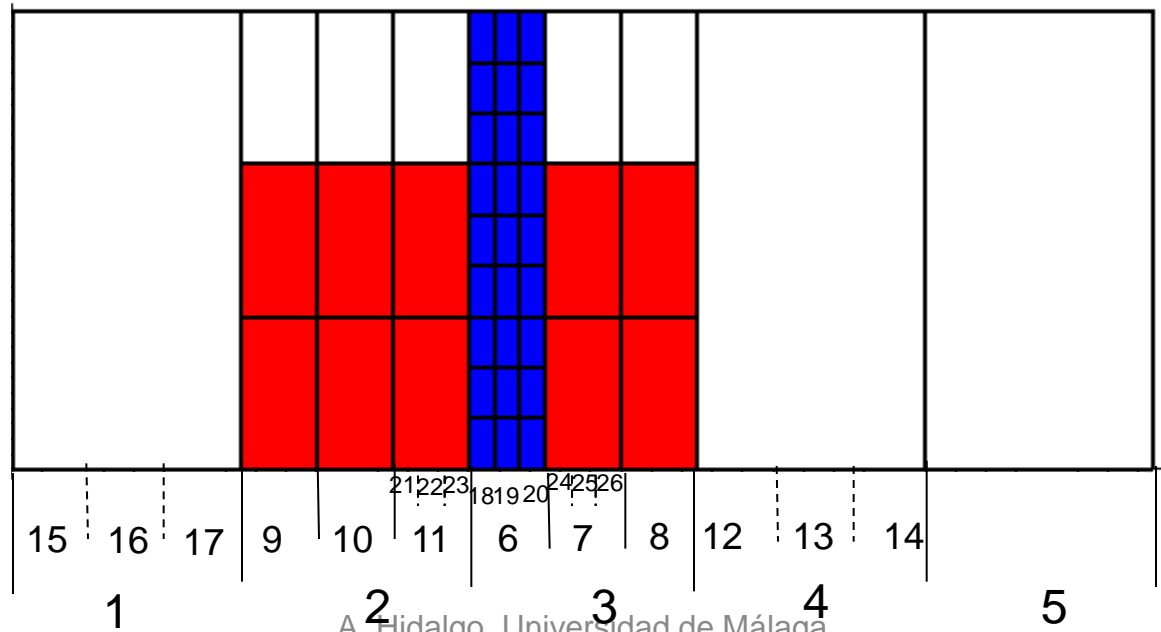


- Regular active
- Virtual coarse
- Virtual refined

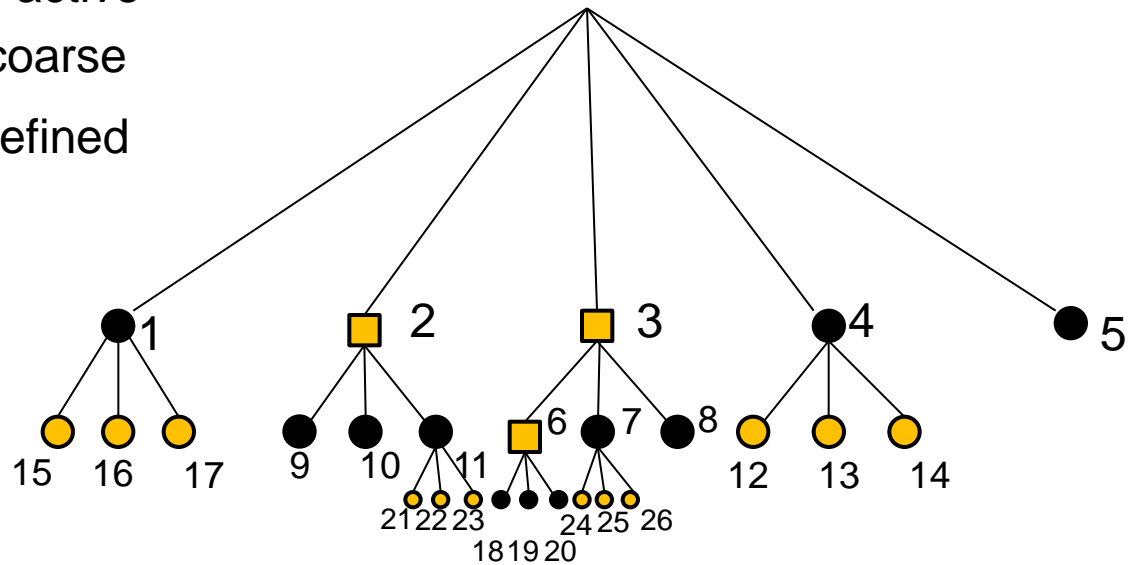


t^{n+1}

t^n

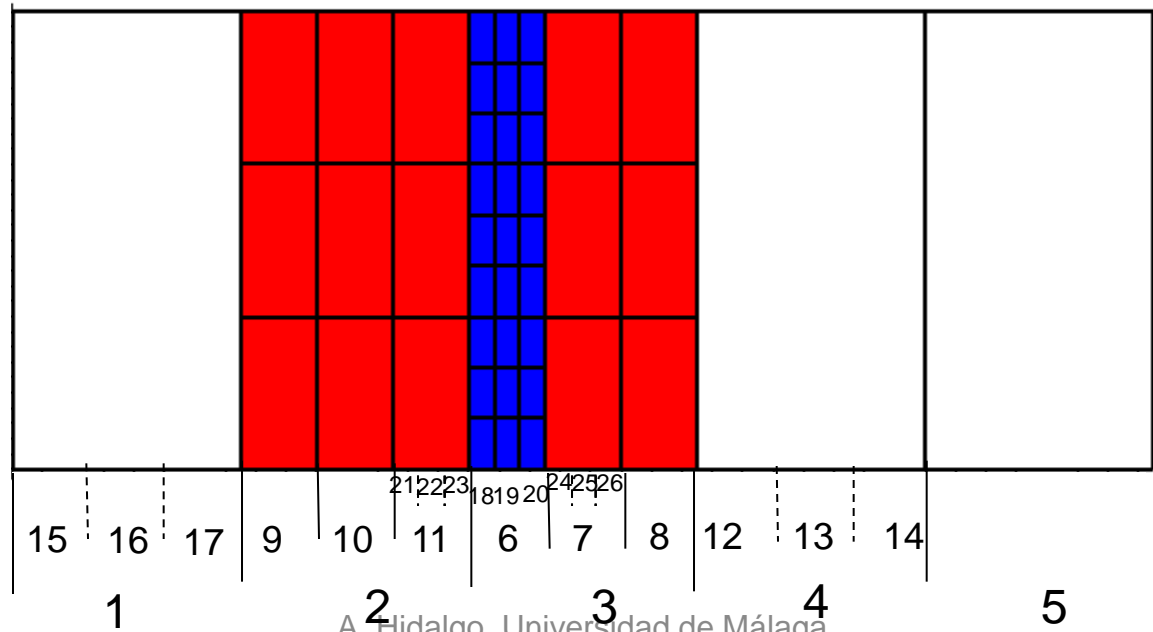


- Regular active
- Virtual coarse
- Virtual refined

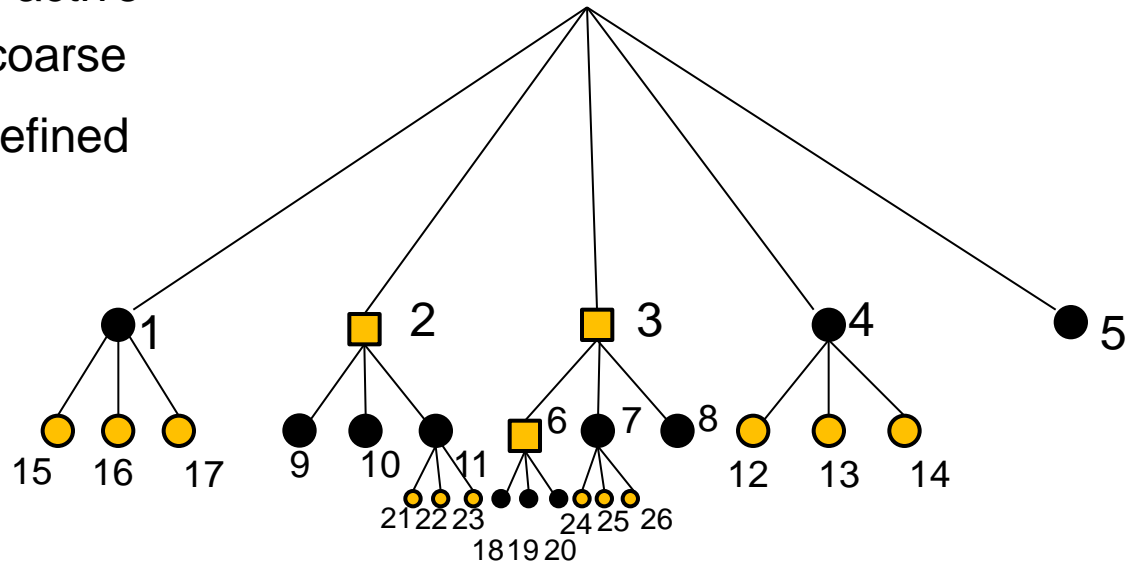


t^{n+1}

t^n

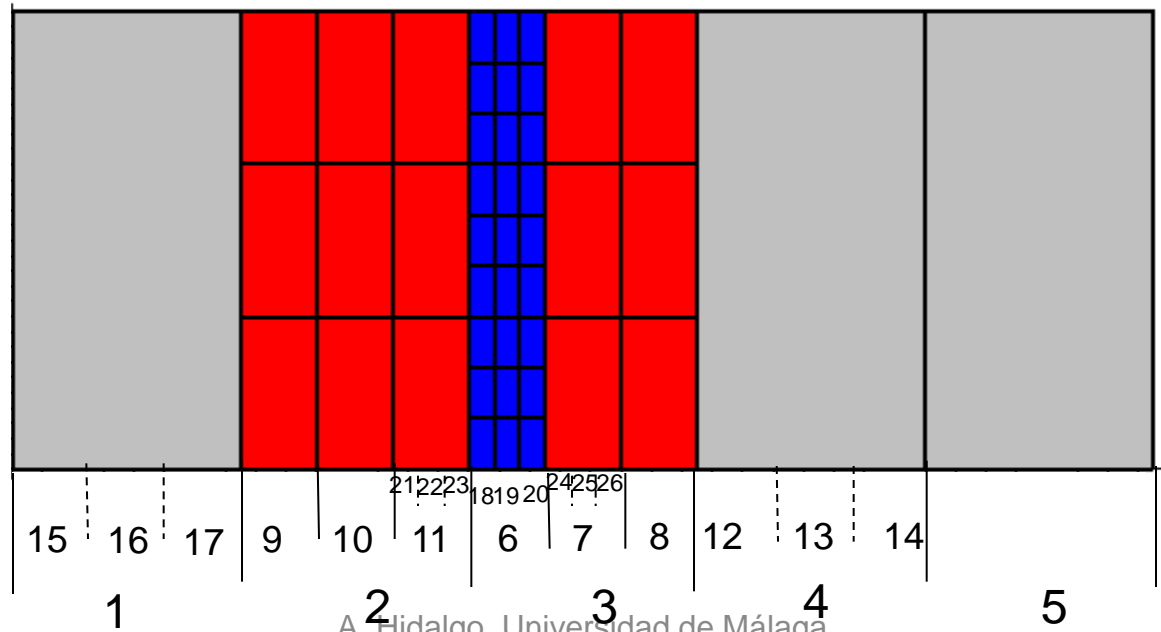


- Regular active
- Virtual coarse
- Virtual refined



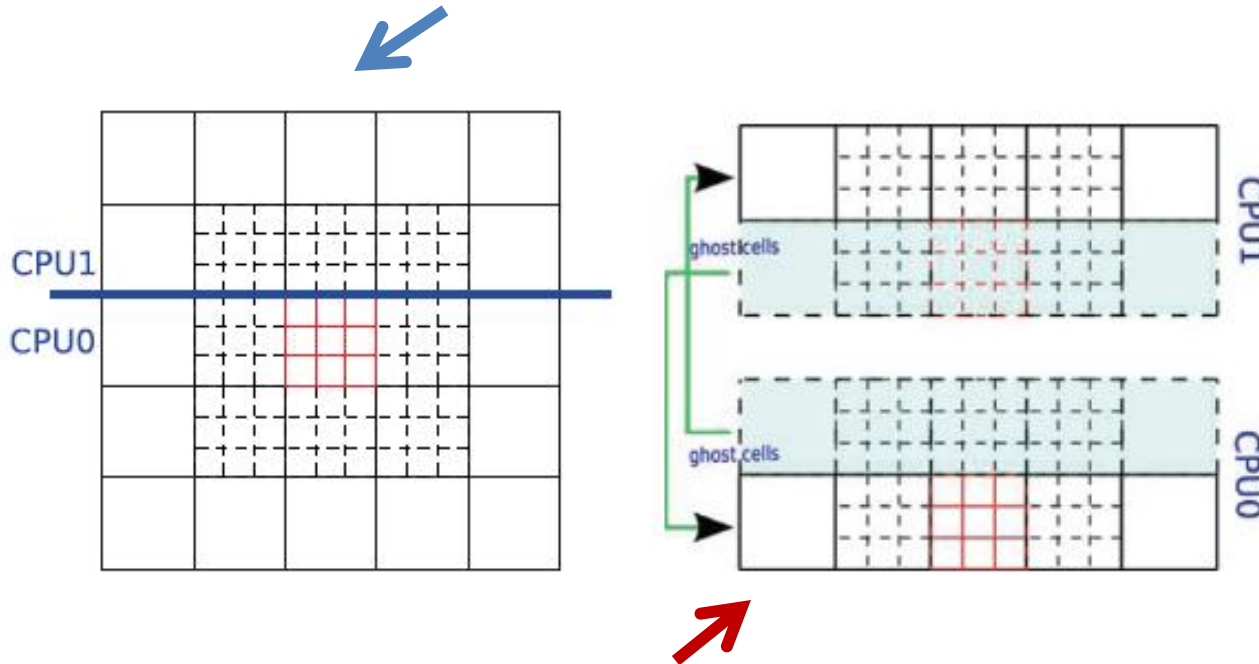
t^{n+1}

t^n



MPI Parallelization

Processors CPU0 and CPU1 exchange information about which cells are refined (full-red) or virtually refined (dashed-black).



CPU₀ informs CPU₁ that a number of real cells in the domain of CPU₁ need virtual refinement.

CPU₁ checks whether such cells have already received an instruction of virtual refinement internal to CPU₁.

We use *exchange lists* to perform the link between the true cells of CPU₀ and those belonging to the MPI-ghost zone of CPU₁.

Each processor has a MPI-ghost zone of cells that are a copy of the true cells managed by the adjacent processor.

NUMERICAL EXAMPLES

Interacting blast waves

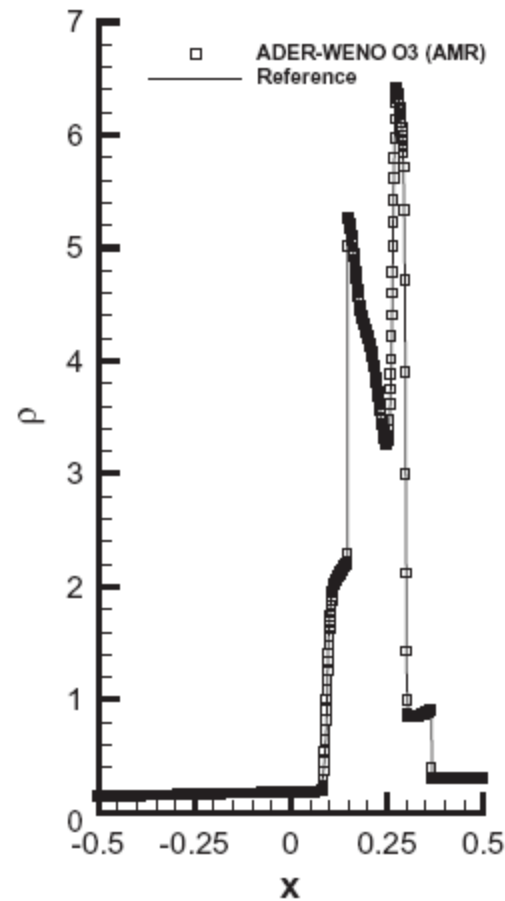
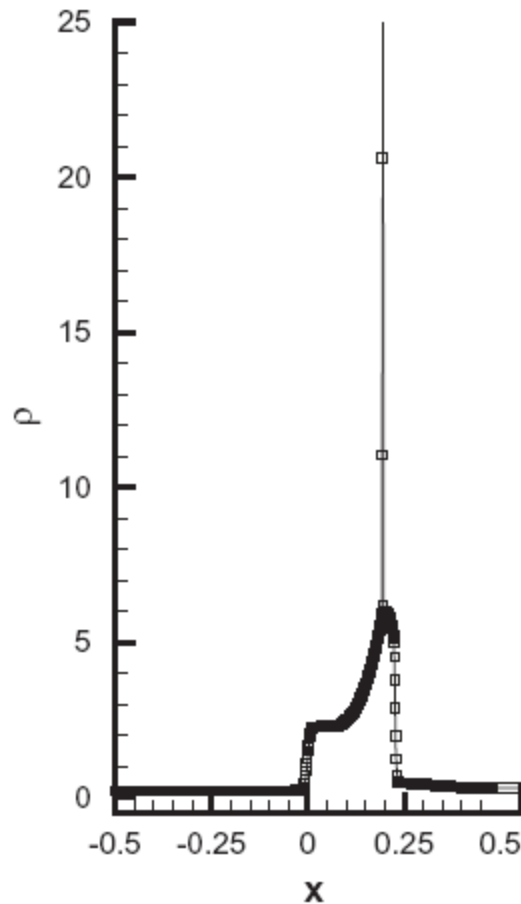
Initial conditions given by

$$(\rho, v_x, p) = \begin{cases} (1.0, 0.0, 10^3) & \text{if } -0.5 < x < -0.4 \\ (1.0, 0.0, 10^{-2}) & \text{if } -0.4 < x < 0.4 \\ (1.0, 0.0, 10^2) & \text{if } 0.4 < x < 0.5 \end{cases}$$

Although 1D, we have evolved this problem in two spatial dimensions over the domain $[-0.5, 0.5] \times [-0.5, 0.5]$, using reflecting boundary conditions in **x direction** and periodic boundary conditions along the **y direction**.

The adiabatic index $\gamma=1.4$.

Originally proposed in P. Woodward, P Colella, *The Numerical Simulation of Two-Dimensional Fluid Flow with Strong Shocks*, Journal of Computational Physics 54, 115.173 (1984)



.Two refinement levels.
 .Ref. sol.: TVD FD
 scheme with 3600 grid
 points

Two waves hit each other from
 opposite directions, producing a very
 strong density peak.

The waves have crossed each other

3D explosion problem

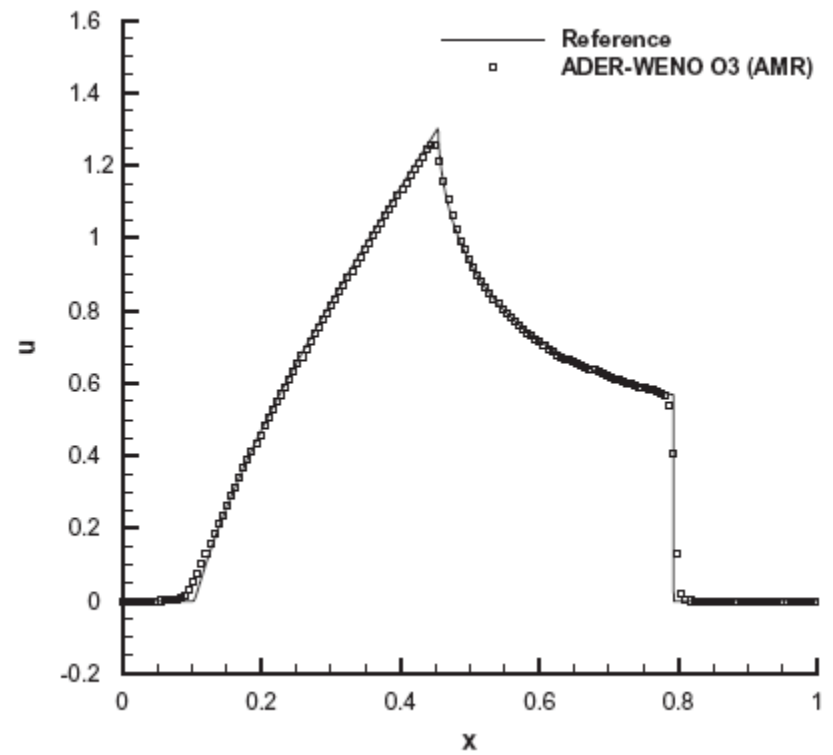
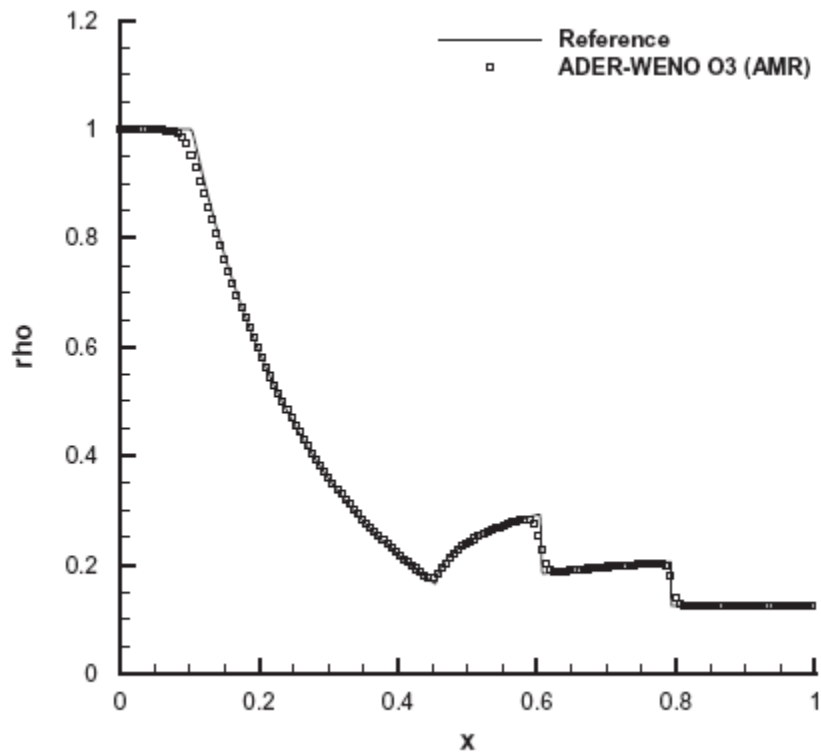
Case	ρ	p	v_x	v_y	v_z	t_e
Inner	1.0	0.0	0.0	0.0	0.0	0.25
Outer	0.125	0.1	0.0	0.0	0.0	

$$u(x,0) = \begin{cases} u_i & \text{if } r \leq R, \\ u_0 & \text{if } r > R \end{cases}$$

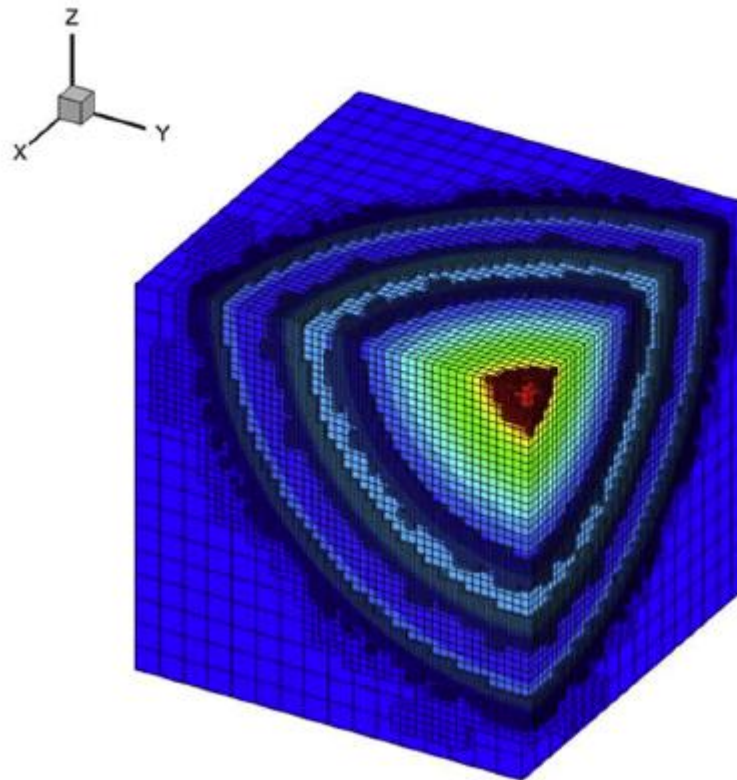
we take here $R=4$

Equivalent 1D problem in radial direction to obtain the referenc solution

$$\frac{\partial}{\partial t} \begin{pmatrix} \rho \\ \rho u \\ E \end{pmatrix} + \frac{\partial}{\partial r} \begin{pmatrix} \rho u \\ \rho u^2 + p \\ u(E + p) \end{pmatrix} = -\frac{d-1}{r} \begin{pmatrix} \rho u \\ \rho u^2 \\ u(E + p) \end{pmatrix}$$



1D cut along x-axis at time = 0.25. Density.



AMR grid structure at time $t=0.25$. Density contour colors

Forward facing step

Another classical test problem for high resolution shock--capturing finite volume scheme consists in the forward facing step problem also called **the Mach 3 wind tunnel test**.

The computational domain is given by $\Omega = [0;3] \times [0;1] \setminus [0.6;3] \times [0;0.2]$

and the initial condition is a uniform flow at Mach number $M=3$ moving to the right.

$$\rho(x,y,0) = 1, \quad p(x,y,0) = 1/\gamma, \quad v_x(x,y,0) = 3 \text{ and } v_y = v_z = 0$$

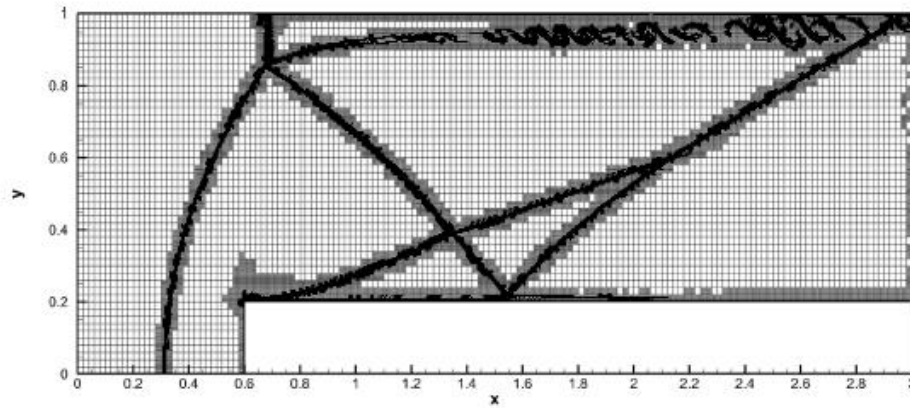
$$\gamma = 1.4$$

Reflective boundary conditions: upper and lower boundary of the domain

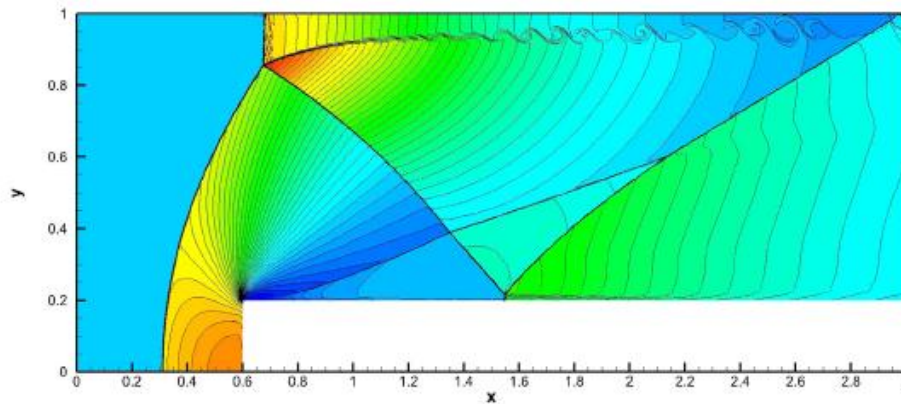
Inflow/outflow boundary conditions: the entrance/exit.

At the corner of the step, there is a singularity.

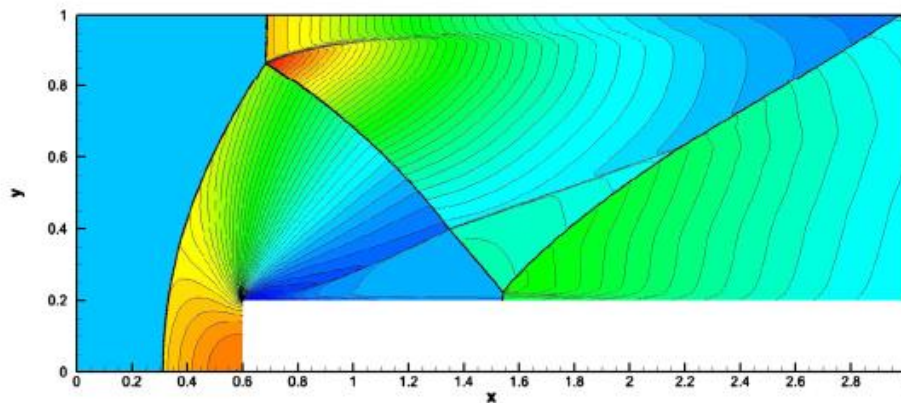
Mesh at the coarsest level: 150x50 cells.



AMR grid



ADER-WENO scheme



Second order solution

MHD equations

Classical, i.e. non-relativistic, equations of ideal magnetohydrodynamics (MHD) in 3D. The MHD system introduces an additional difficulty for numerical schemes since the **divergence of the magnetic field must remain zero for all times**

$$\frac{\partial B_x}{\partial x} + \frac{\partial B_y}{\partial y} + \frac{\partial B_z}{\partial z} = 0$$

We use the hyperbolic version of the generalized Lagrangian multiplier (GLM) divergence cleaning approach proposed in Dedner et al JCP(2002) : adding an auxiliary variable ψ and one linear scalar PDE to the MHD system to transport divergence errors out of the computational domain with the artificial speed c_h

$$\frac{\partial \mathbf{u}}{\partial t} + \text{div}(\mathbf{F}) = 0 \quad \mathbf{u}^T = \left(\rho \quad \rho \vec{v}^T \quad E \quad \vec{B}^T \quad \psi \right)$$

$$\mathbf{F} = \begin{pmatrix} \rho \vec{v}^T \\ \rho \vec{v} \vec{v} + \left(p + \frac{1}{8\pi} \vec{B}^2 \right) \mathbf{I} - \frac{1}{4\pi} \vec{B} \vec{B} \\ \vec{v}^T \left(E + p + \frac{1}{8\pi} \vec{B}^2 \right) - \frac{1}{4\pi} \vec{B}^T (\vec{v} \cdot \vec{B}) \\ \vec{v} \vec{B} - \vec{B} \vec{v} + \psi \mathbf{I}, \\ c_h^2 \vec{B}^T \end{pmatrix}$$

Equation of state is the ideal gas law:

$$p = (\gamma - 1) \left(E - \frac{1}{2} \rho \vec{v}^2 - \frac{\vec{B}^2}{8\pi} \right)$$

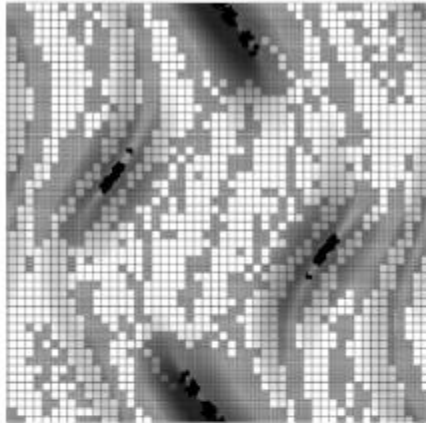
Orszag-Tang vortex system

The Orszag-Tang Vortex is a well-known test for MHD codes. The initial conditions lead to a system of supersonic MHD turbulence, making this problem a good test of the algorithm's ability to handle such turbulence and MHD shocks. Furthermore, given the set up described here, the problem is symmetric under a rotation of 180° , providing a symmetry test for the MHD version of the algorithm.

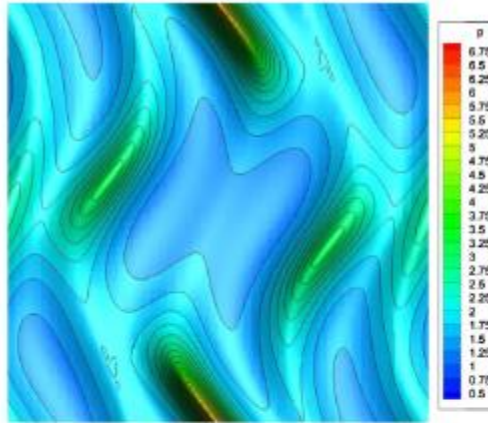
$$(\rho, u, v, p, B_x, B_y) = (\gamma^2, -\sin(y), \sin(x), \gamma, -\sqrt{4\pi} \sin(y), \sqrt{4\pi} \sin(2x)),$$

$$w = B_z = 0; \gamma = \frac{5}{3}; c_h = 2.0$$

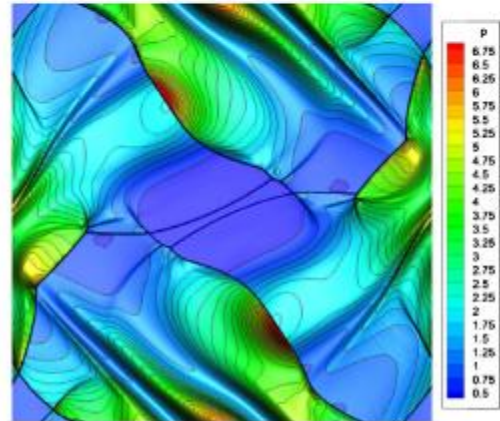
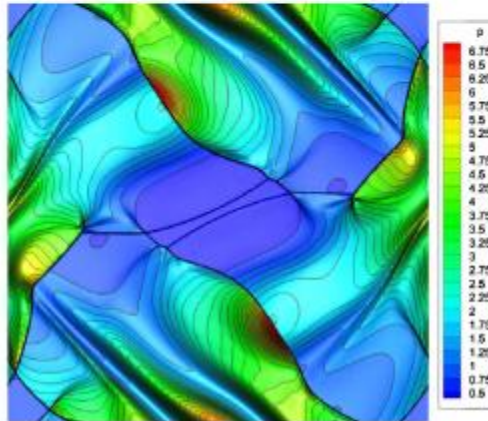
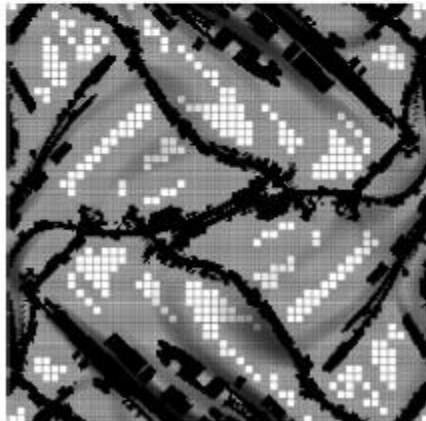
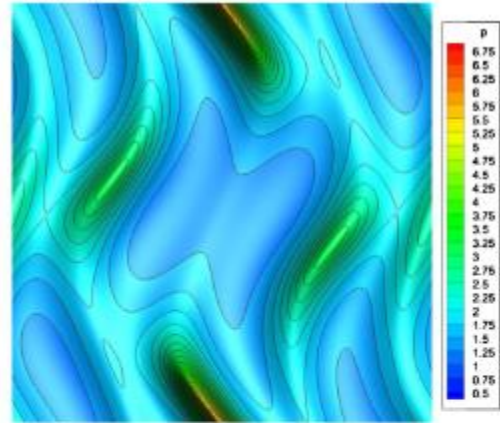
AMR grid



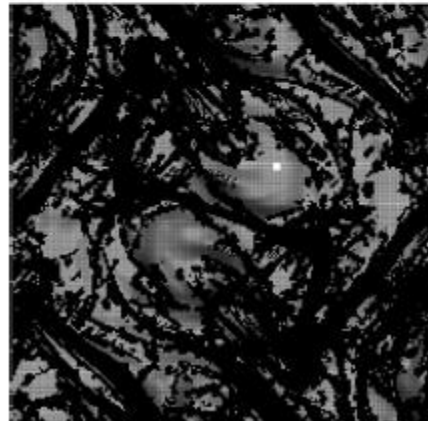
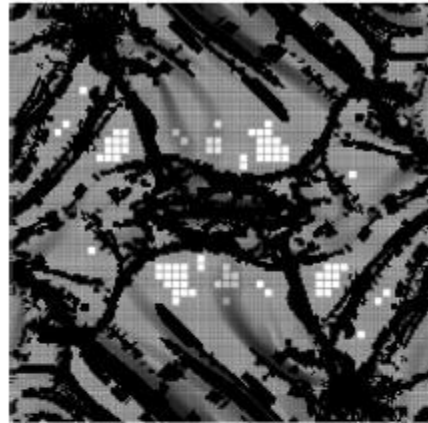
AMR O3



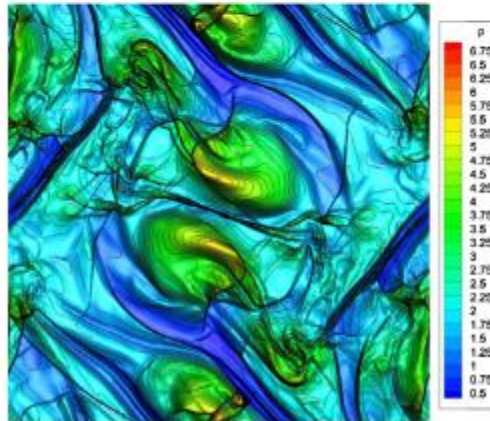
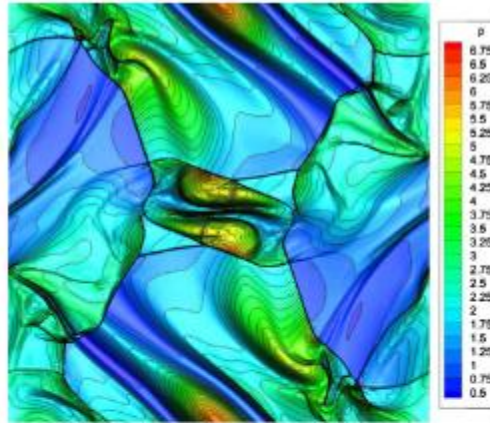
Uniform-finer grid



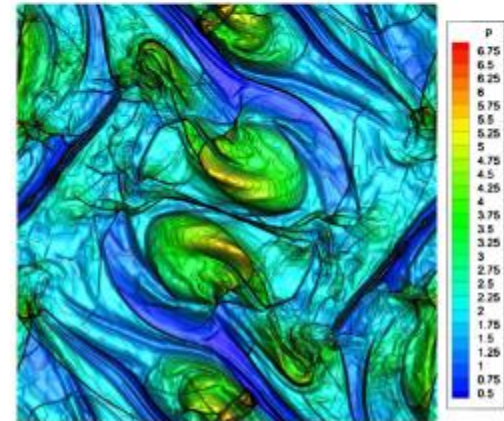
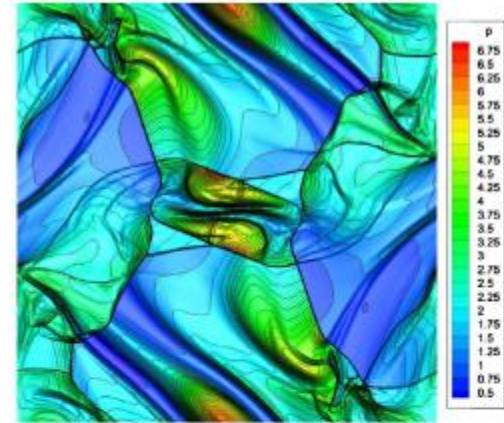
AMR grid



AMR O3



Uniform-finer grid



	AMR	Uniform	Ratio
Cells	454,525	640,000	1.41
CPU	0.547	1.0	1.83

Rotor problem

A rapidly rotating fluid of high density embedded in a fluid at rest with low density.

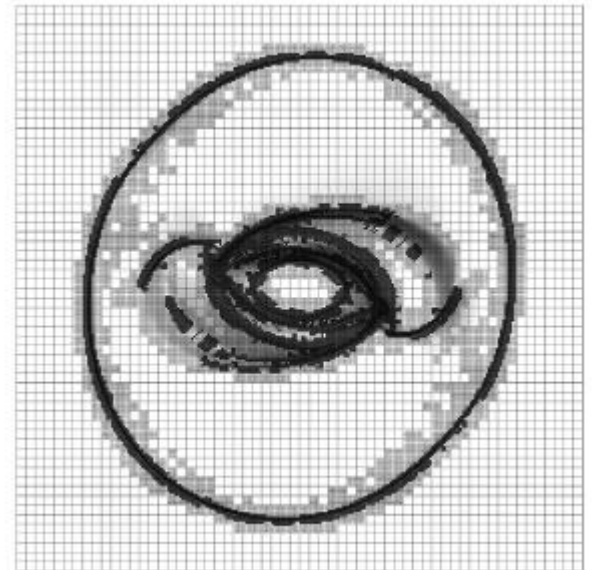
Both fluids are subject to an initially constant magnetic field. The rotor causes torsional Alfvén waves to be launched into the fluid at rest. As a result the angular momentum of the rotor is diminished.

$$\rho(x,0) = \begin{cases} 10 & \text{if } r \in [0,0.1], \\ 1 & \text{ambient fluid} \end{cases}$$

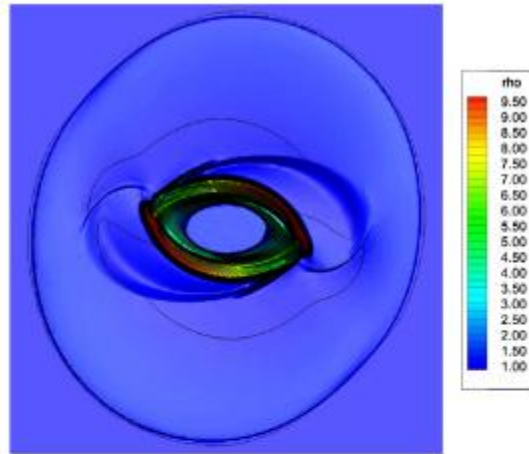
$$v = \omega r = 1 \quad \text{at } r = 0.1$$

Pressure $p=1$, magnetic field vector: $\mathbf{B} = (2.5, 0, 0)^T$
in the entire domain

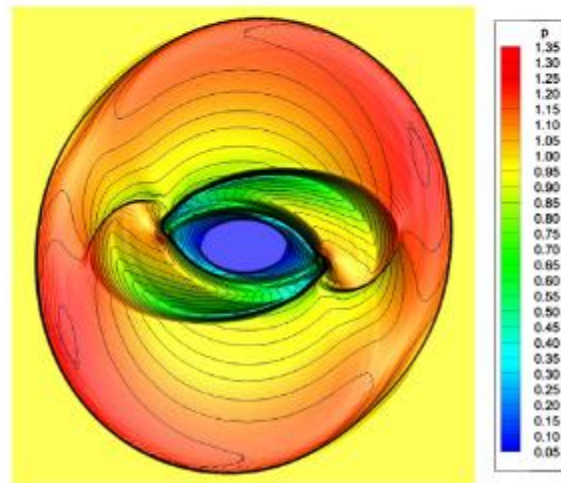
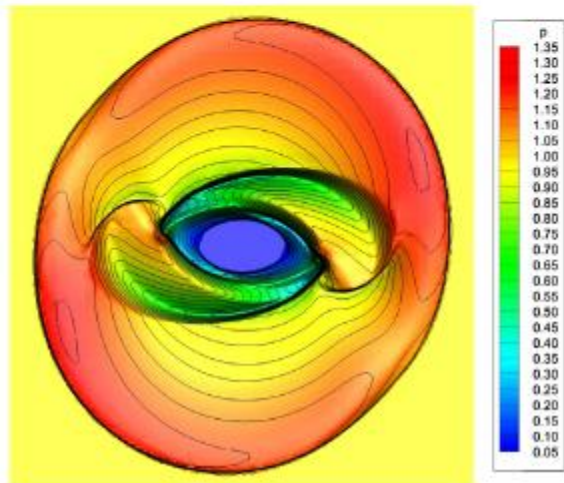
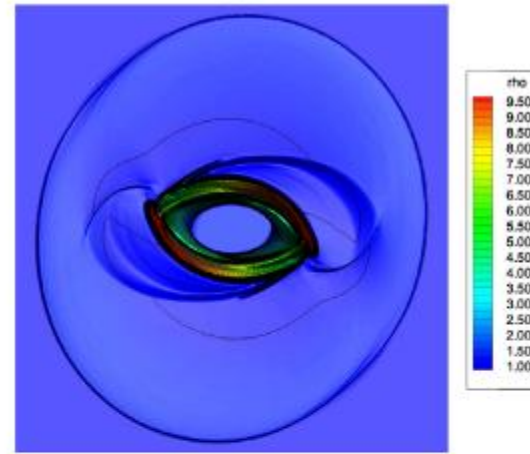
Originally proposed by Balsara & Spicer, JCP (1999)



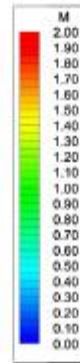
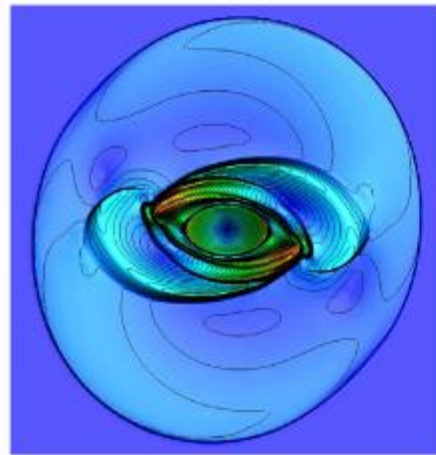
AMR O3



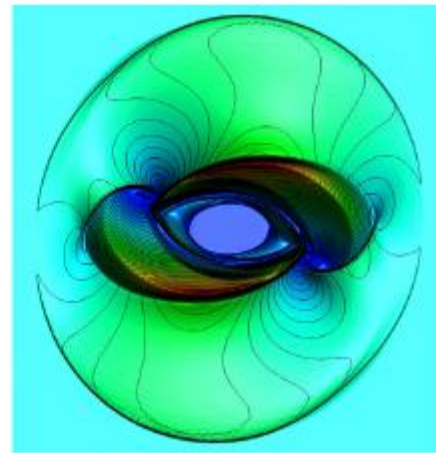
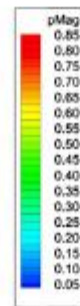
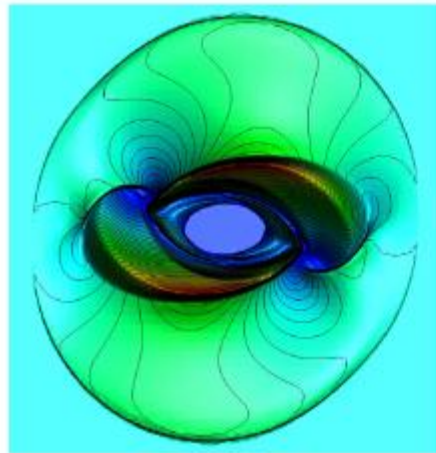
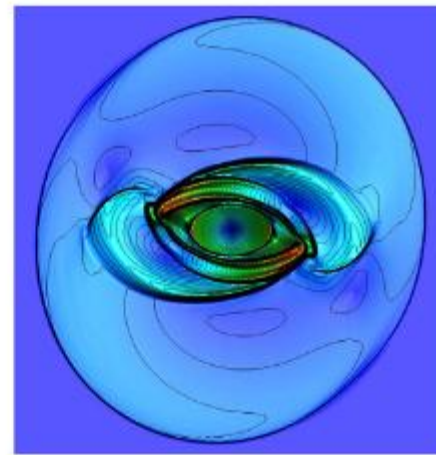
Uniform-finer grid



AMR O3



Uniform-finer grid



	AMR	Uniform	Ratio
Elements	179,680	921,600	5.13
CPU time	0.140	1.0	7.14

REFERENCES

Michael Dumbser, Olindo Zanotti, Arturo Hidalgo, Dinshaw S. Balsara
(2013). *ADER-WENO finite volume schemes with space–time adaptive mesh refinement*.
JCP 248 pp 257-286.

For the non conservative case:

Michael Dumbser, Arturo Hidalgo, Olindo Zanotti
(2014). *High order space–time adaptive ADER-WENO finite volume schemes for non-conservative hyperbolic systems* . CMAME 268, pp 359-387.

REFERENCES

Michael Dumbser, Olindo Zanotti, Arturo Hidalgo, Dinshaw S. Balsara
(2013). *ADER-WENO finite volume schemes with space–time adaptive mesh refinement*.
JCP 248 pp 257-286.

For the non conservative case:

Michael Dumbser, Arturo Hidalgo, Olindo Zanotti
(2014). *High order space–time adaptive ADER-WENO finite volume schemes for non-conservative hyperbolic systems*. CMAME 268, pp 359-387.

¡ MUCHAS GRACIAS !